

Alma Mater Studiorum Università di Bologna  
Archivio istituzionale della ricerca

Advection pathways at the Mt. Cimone WMO-GAW station: Seasonality, trends, and influence on atmospheric composition

This is the final peer-reviewed author's accepted manuscript (postprint) of the following publication:

*Published Version:*

E. Brattich, J.A.G.Orza, P. Cristofanelli, P. Bonasoni, A. Marinoni, L. Tositti (2020). Advection pathways at the Mt. Cimone WMO-GAW station: Seasonality, trends, and influence on atmospheric composition. *ATMOSPHERIC ENVIRONMENT*, 234, 1-18 [10.1016/j.atmosenv.2020.117513].

*Availability:*

This version is available at: <https://hdl.handle.net/11585/760791> since: 2021-01-29

*Published:*

DOI: <http://doi.org/10.1016/j.atmosenv.2020.117513>

*Terms of use:*

Some rights reserved. The terms and conditions for the reuse of this version of the manuscript are specified in the publishing policy. For all terms of use and more information see the publisher's website.

This item was downloaded from IRIS Università di Bologna (<https://cris.unibo.it/>).  
When citing, please refer to the published version.

(Article begins on next page)

This is the final peer-reviewed accepted manuscript of:

E. Brattich, J.A.G. Orza, P. Cristofanelli, P. Bonasoni, A. Marinoni, L. Tositti, *Advection pathways at the Mt. Cimone WMO-GAW station: Seasonality, trends, and influence on atmospheric composition*, Atmospheric Environment, Volume 234, 2020, 117513.

The final published version is available online at:  
<https://doi.org/10.1016/j.atmosenv.2020.117513>

Rights / License:

The terms and conditions for the reuse of this version of the manuscript are specified in the publishing policy. For all terms of use and more information see the publisher's website.

This item was downloaded from IRIS Università di Bologna (<https://cris.unibo.it/>)

**When citing, please refer to the published version.**

1 **Advection pathways at the Mt. Cimone WMO-GAW station: seasonality,**  
2 **trends, and influence on atmospheric composition.**

3  
4 **E. Brattich<sup>1</sup>, J.A.G. Orza<sup>2</sup>, P. Cristofanelli<sup>3</sup>, P. Bonasoni<sup>3</sup>, A. Marinoni<sup>3</sup>, L. Tositti<sup>4</sup>**

5 <sup>1</sup> Department of Physics and Astronomy DIFA, Alma Mater Studiorum University of Bologna,  
6 40126 Bologna (BO), Italy.

7 <sup>2</sup> SCOLAb, Fisica Aplicada, Miguel Hernandez University, 03202 Elche, Spain.

8 <sup>3</sup> ISAC-CNR, Via Piero Gobetti, Bologna (BO), Italy.

9 <sup>4</sup> Environmental Chemistry and Radioactivity Laboratory, Department of Chemistry “G.  
10 Ciamician”, Alma Mater Studiorum University of Bologna, 40126 Bologna (BO), Italy.

11  
12 Corresponding author: Erika Brattich ([erika.brattich@unibo.it](mailto:erika.brattich@unibo.it))

13  
14  
15 **Keywords:** back-trajectories; teleconnection; trends; aerosol; atmospheric radiotracers.

16 **Highlights:**

- 17 • Characterisation of primary advection pathways to the Mt. Cimone baseline station  
18 • Characterisation of atmospheric constituents by advection pathway to Mt. Cimone  
19 • Trend analysis of atmospheric pathways and atmospheric composition at Mt. Cimone  
20 • Associations between pathways, atmospheric composition and teleconnection indices  
21

## 22 Abstract

23 Relationships are analysed between advection pathways and atmospheric composition at the  
24 high-mountain station of Mt. Cimone (Italy), between 1999 and 2006. Back-trajectory cluster  
25 analysis identifies eight main advection pathways. A connection is demonstrated between the  
26 seasonality of air mass transport and atmospheric composition. Temporal trends and correlation  
27 of variables, flow types and teleconnection indices show, among other, decreasing trends of  $^{210}\text{Pb}$   
28 (a radionuclide of crustal origin;  $-0.008 \text{ mBq m}^{-3} \text{ year}^{-1}$ ) as well as  $\text{PM}_{10}$  ( $-0.15 \mu\text{g m}^{-3} \text{ year}^{-1}$ ),  
29 indicating that previously observed downward  $\text{PM}_{10}$  trends in Europe may actually be  
30 attributable to a combination of meteorological factors and decreasing anthropogenic emissions.  
31 The detection of a positive (negative) correlation of these tracers with Western (Arctic) air  
32 masses, showing significant downward (upward) trends at the study site, further confirms our  
33 findings. Lastly, relationships between teleconnection indices and atmospheric transport  
34 types/atmospheric variables are further analysed, focusing on large-scale atmospheric circulation  
35 indices and regional low-frequency atmospheric circulation pathways, the Mediterranean  
36 Oscillation and the Western Mediterranean Oscillation. The analysis reveals the important  
37 influence of such regional indices on the advection pathways.

## 38 1 Introduction

39 There is a pressing need to improve understanding of processes contributing the seasonal  
40 variability of background/baseline (i.e. well-mixed tropospheric) atmospheric composition in the  
41 central north Mediterranean region, a hotspot of air pollution and climate change. In fact, due to  
42 the sunny, hot and dry weather typical of this region especially during summer, together with the  
43 convergence of long-range transport over the basin, air pollution in the form of reactive  
44 compounds is often higher than in most European inland regions (Dulac et al., 2016). In addition,  
45 climate change will significantly impact air quality with numerous two-way interactions not  
46 always well understood.

47 Air pollution in the Mediterranean basin is primarily in the form of particulate matter and ozone  
48 and nitrogen deposition (Ochoa-Hueso et al., 2017).

49 In this framework, clustering of backward trajectories has been used to study the influence of the  
50 origin and pathway of air masses on composition change (for a review see Fleming et al., 2012).  
51 The investigation of vertical motions in the atmosphere may take advantage of using  $^7\text{Be}$  and  
52  $^{210}\text{Pb}$  radiotracers, because of their naturally contrasting origin: in fact,  $^7\text{Be}$  (half-life 53.3 days)  
53 is produced by cosmic ray spallation reactions with nitrogen and oxygen in the stratosphere  
54 (about 75%) and in the upper troposphere (Usoskin and Kovaltsov, 2008), while  $^{210}\text{Pb}$  (half-life  
55 22 years) is a tracer of continental air masses (Balkanski et al., 1993), being emitted as decay  
56 product of  $^{222}\text{Rn}$  (half-life 3.8 days) deriving from crustal rocks and soils (Turekian et al., 1977).  
57 Once produced, both radionuclides attach to submicron-sized aerosol particles peaking in the  
58 accumulation mode (e.g., Gaffney et al., 2004). Thereafter, the main removal mechanisms of  $^7\text{Be}$   
59 and  $^{210}\text{Pb}$  from the atmosphere are wet and dry scavenging of the carrier aerosol (Feely et al.,  
60 1989; Kulan et al., 2006). For this reason, simultaneous measurements of  $^7\text{Be}$  and  $^{210}\text{Pb}$ , and  
61 analysis of their ratio, can provide useful information about the vertical motion of air masses as  
62 well as on convective activity in the troposphere (e.g., Koch et al., 1996; Lee et al., 2007).

63 The use of air mass classification together with atmospheric radiotracers is not common, but  
64 has been the subject of some studies (e.g. Arimoto et al., 1999; Hernández et al., 2008; Dueñas  
65 et al., 2011; Lozano et al., 2012; Chambers et al., 2013, 2014, 2016 a,b; Grossi et al., 2016;  
66 Hernández-Ceballos et al., 2016). However, most of the previous studies of this kind in the

67 Mediterranean region focused on relatively short time series, and focused on understanding the  
68 variability of atmospheric radiotracers without a clear connection to other atmospheric  
69 compounds. Moreover, while the relation between natural radionuclides and teleconnection  
70 indices has been the subject of recent studies (Grossi et al., 2016; Sarvan et al., 2017), the  
71 variability in the occurrence of each trajectory group and the assessment of trends in association  
72 with large-scale atmospheric circulation indices, such as the North Atlantic Oscillation index  
73 (NAOi), is less common (Orza et al., 2013). Even less studied is the association in the  
74 occurrence of advection pathways with the remaining modes of atmospheric circulation over  
75 Europe, such as the Eastern Atlantic (EA) pattern, Eastern Atlantic/Western Russia (EA/WR),  
76 and the Scandinavian (SCA) pattern. Together with NAO, these indices represent the most  
77 important mid-latitude modes for the Mediterranean climate at the monthly time scale (Trigo et  
78 al., 2006).

79 In this context, long-term measurements at the high-elevation WMO-GAW baseline station  
80 of Mt. Cimone (Italy; 44°11' N, 10°42' E, 2165 m asl) are of paramount importance. In  
81 particular, they are useful for the identification of dominant advection pathways, assessing  
82 associations between pathways and atmospheric composition, and investigating links between  
83 flow pathways and circulation modes in the Mediterranean region on seasonal and interannual  
84 time scales. In addition, the occurrence of trends and the relationships of trends in atmospheric  
85 composition with those in advection pathways and teleconnection indices in the monthly time  
86 series are also explored, focusing not only on large-scale indices but considering two additional  
87 regional low-frequency atmospheric circulation pathways, namely the Mediterranean Oscillation  
88 (MO) and the Western Mediterranean Oscillation (WeMO). It should be emphasized here that,  
89 historically, the investigation of atmospheric circulation model influences (both large-scale and  
90 regional) typically focused on precipitation and temperature pathways. To date, there has been  
91 limited exploration of the relationship between these modes and advection pathways/atmospheric  
92 composition.

93 This work is organized as follows. We first describe the measurement techniques and the  
94 statistical methods used. We then present and discuss our results on: 1) the description of the  
95 main advection pathways found by the cluster analysis of back trajectories; 2) the analysis of the  
96 relationships between advection pathways and meteorological parameters/other atmospheric  
97 components; 3) the temporal analysis of the monthly time series, including trends; 4) the  
98 associations of air flow types with teleconnection indices and meteorological/atmospheric  
99 variables. We finally summarize our main conclusions.

## 100 **2 Materials and Methods**

### 101 **2.1 Sampling site**

102 Mt. Cimone, the highest peak of the Italian northern Apennines, hosts a global station of the  
103 Global Atmosphere Watch (GAW) programme of the World Meteorological Organization  
104 (WMO) constituted by a meteorological observatory by the Italian Air Force (active since 1941)  
105 and a research facility managed by the Institute of Atmospheric Sciences and Climate (ISAC) of  
106 the National Research Council of Italy (CNR), active since 1996. The site is located far away  
107 from large industrialized and urban areas, has a 360° free horizon experiencing both regional and  
108 long-range transport of air masses (Bonasoni et al., 1999, 2000b; Cristofanelli et al., 2006,  
109 2009a, b, 2013; Cristofanelli and Bonasoni, 2009; Tositti et al., 2013). The elevation of the site  
110 (2165 m asl) is such that the station lies above the planetary boundary layer (PBL) during most  
111 of the year, even if an influence of the innermost layer is evident during warm months due to the

112 increased mixing height and the influence of the mountain/valley breeze regimes (Fischer et al.,  
113 2003; Cristofanelli et al., 2007; Griffiths et al., 2014). For these reasons, under specific conditions  
114 (i.e. usually during cold months and during stable summer nights when regional anti-cyclonic  
115 conditions dominate), the measurements of atmospheric compounds and meteorological  
116 parameters at this site can be considered representative of the well-mixed southern European-  
117 Mediterranean basin free troposphere (Bonasoni et al., 2000a; Fischer et al., 2003; Cristofanelli et  
118 al., 2007, 2018), a region which is recognized as a hot-spot both in terms of climate change and  
119 air quality.

## 120 121 **2.2 Measurements**

122 As a WMO-GAW station, several atmospheric compounds have been measured at Mt.  
123 Cimone for many years (Cristofanelli et al., 2018): CO<sub>2</sub> (since 1979) (Ciattaglia, 1983, 1986;  
124 Colombo et al., 2000), tropospheric O<sub>3</sub> (since 1991) (Cristofanelli et al., 2015, 2018),  
125 concentration and size distribution of particles with optical diameter between 0.30 and 20 µm  
126 (since 2000) (Marinoni et al., 2008), black carbon (July 2005) (Marinoni et al., 2008), and CO  
127 (since 2007) (Cristofanelli et al., 2009b).

128 <sup>7</sup>Be, <sup>210</sup>Pb and aerosol mass loading in the form of PM<sub>10</sub> (airborne particulate matter with a  
129 mean aerodynamic diameter less than 10 µm) were measured regularly in the period 1998-2011  
130 with a Thermo-Environmental PM<sub>10</sub> high-volume sampler (average flow rate of 1.13 m<sup>3</sup> min<sup>-1</sup> at  
131 standard temperature and pressure conditions) (Lee et al., 2007; Tositti et al., 2012, 2013, 2014).

132 After retrieval, the observations of the various atmospheric parameters previously mentioned,  
133 as well as of meteorological parameters such as temperature, pressure, relative humidity, and  
134 wind speed, were averaged to the same time resolution of PM<sub>10</sub> and atmospheric radionuclides  
135 for statistical homogenization of data. In fact, as the PM<sub>10</sub> filters at the station are manually  
136 changed, sampling time is not uniform. Anyway as most of the samples were collected over 48  
137 hours (sampling approximately 3250 m<sup>3</sup> of air), in order to safely apply statistical techniques,  
138 data have been firstly homogenized by selecting only those samples which collected a volume  
139 between 2700 and 3700 m<sup>3</sup>.

140 We also included tropopause heights in the analysis, calculated from the radiosoundings in  
141 San Pietro Capofiume (44°39'N, 11°37'E, 10m a.s.l.), a regional meteorological station located  
142 in the Po Valley to the North-East of Mt. Cimone, available since 1987 from the University of  
143 Wyoming website (<http://weather.uwyo.edu/upperair/sounding.html>).

## 144 145 **2.3 Teleconnection indices**

146 As reported in the Introduction, here we investigate the connection of atmospheric composition  
147 and advection pathways with teleconnection indices, considering both large-scale and regional  
148 scale teleconnections, i.e. NAO, EA, EA/WR, SCA, MO, and WeMO. Table 1 presents an  
149 overview of the teleconnections investigated in this paper.

150 The NAO, a redistribution of atmospheric mass between the Arctic and the subtropical  
151 Atlantic (Hurrell, 1995), has been identified as the dominant mode of variability of the surface  
152 atmospheric circulation across the Atlantic (Barnston and Livezey, 1997). The NAO is  
153 determined by the position and strength of the Icelandic low and the Bermuda-Azores High.  
154 Oscillations between high and low NAO phases modulate the westerly jet stream and cause large  
155 changes in the heat and moisture transport between the Atlantic and the neighbouring continents  
156 (e.g., Hurrell, 1995, 1996), affecting the intensity and number of storms (Hurrell et al., 2003).  
157 These changes influence air pollutant transport and dispersion, impacting, for instance, the

158 transport of Saharan dust into the Mediterranean and Atlantic in winter (Moulin et al., 1997), the  
159 export and import pathways of pollution to the Mediterranean basin (Hurrell, 1995), influencing  
160 local-to-regional scale pollutant concentrations (e.g., Cuevas et al., 2013; Cristofanelli et al.,  
161 2015), and modifying the transport of pollutants from North America to Europe (Li et al., 2002).  
162 A relation between the NAO phase and Stratosphere-to-Troposphere Transport (STT) variability  
163 has also been pointed out (James et al., 2003; Cristofanelli et al., 2006, 2015). A common  
164 measure of the NAO phase is the so-called NAO index (NAOi) which is commonly defined as  
165 the difference in normalized sea level pressure (SLP) anomalies between either Lisbon (Portugal)  
166 or Ponte Delgada (Azores), and Stykkisholmur/Reykjavik (Iceland) (Hurrell, 1995). Alternative  
167 definitions of NAOi have been introduced, including one based on the empirical orthogonal  
168 function (EOF) analysis of the SLP field. The NAOi in this case is identified as the leading  
169 eigenvector (the first Principal Component, PC1) computed from the time variation of the SLP  
170 field (e.g., Hurrell et al., 2003). The advantage of using EOF analysis of the SLP field is that the  
171 PC1 provides a more accurate representation of the NAO pattern considering the shifting of the  
172 NAO centres of action throughout the year (Pausata et al., 2012). This index appears to be less  
173 noisy than the station-based indices. Both monthly indices present a significant correlation  
174 coefficient equal to 0.80 and 0.76 over the periods 1998-2011 and 1999-2006 used in this work,  
175 respectively. Another alternative NAO index, the CRU station-based NAOi, is calculated as the  
176 difference between the normalised SLP over Gibraltar and the normalised SLP over southwest  
177 Iceland (Jones et al., 1997). CRU station-based index presents a significant correlation  
178 coefficient with the previous ones (equal to 0.79 with Hurrell station-based NAOi, and equal to  
179 0.77 with Hurrell principal components-based NAOi).

180 The EA pattern is the second prominent mode of low-frequency variability over the  
181 North Atlantic, and was first described by Wallace and Gutzler (1981) as anomalously high 500  
182 mb height anomalies over the subtropical North Atlantic and eastern Europe when in positive  
183 mode. It consists of a north-south dipole of anomaly centers spanning the North Atlantic from  
184 east to west. The positive phase of the EA pattern is associated with above-average surface  
185 temperatures in Europe in all months and it has been suggested to play a role in positioning the  
186 primary North Atlantic storm track (e.g., Seierstad et al., 2007) and in modulating the location  
187 and strength of the NAO dipole (Hurrell and Deser, 2009).

188 The EA/WR pattern (Lim, 2015) affects Eurasia throughout the year and consists of four  
189 main anomaly centers. The positive phase is associated with positive height anomalies located  
190 over Europe and northern China, and negative height anomalies located over the central North  
191 Atlantic and north of the Caspian Sea.

192 The SCA pattern (Bueh and Nakamura, 2007) consists of a primary circulation center  
193 over Scandinavia, with weaker centers of opposite sign over western Europe and eastern Russia/  
194 western Mongolia. The positive phase of this pattern is associated with positive height  
195 anomalies, sometimes reflecting major blocking anticyclones over Scandinavia and western  
196 Russia, while the negative phase of the pattern is associated with negative height anomalies in  
197 these regions.

198 The MO is a low-frequency variability pattern producing opposing barometric, thermal  
199 and pluviometric anomalies between the western and eastern borders of the Mediterranean basin.  
200 The MO was originally defined as the difference of standardised geopotential height anomalies  
201 at Algiers (Alger) and Cairo (Egypt) (Conte et al., 1989), while similar indices have been defined  
202 in terms of the difference of standardised pressure anomalies at Gibraltar (Spain) and Lod  
203 (Israel) (Palutikof, 2003) or at Marseilles (France) and Jerusalem (Israel) (Brunetti et al., 2002).

204 It has a significant influence over rainfall in the Mediterranean basin (e.g., Martin-Vide and  
205 Lopez-Bustins, 2006; Angulo-Martínez and Beguería, 2012). The WeMO was defined within the  
206 synoptic framework of the Western Mediterranean basin and its vicinities (Martin-Vide and  
207 Lopez-Bustins, 2006). It is defined as the difference between the standardized surface pressure  
208 values in Padua (Italy), and San Fernando (Cadiz, Spain): while the north of Italy is an area with  
209 a relatively high barometric variability due to the influence of the central European anticyclone  
210 and the Liguria low, the gulf of Cadiz is often influenced by the Azores anticyclone. Similar to  
211 MO, WeMO has an important effect on precipitation in the Mediterranean, and especially in the  
212 eastern Iberian Peninsula (e.g., Martin-Vide and Lopez-Bustins, 2006; Angulo-Martínez and  
213 Beguería, 2012; Izquierdo et al., 2013), where NAO is weakly correlated with precipitation.

214

#### 215 **2.4 Clusters of back trajectories, significant differences and trends**

216 In order to analyse the origin of air masses arriving at the measurement site, 96-hour 3D  
217 kinematic back-trajectories starting four times a day (00, 06, 12, 18 UTC) at three heights (1400,  
218 2200 and 3000 m asl) were calculated with the HYbrid Single-Particle Lagrangian Integrated  
219 Trajectory (HYSPLIT) model version 4.8 (Draxler and Hess, 1997, 1998; Draxler, et al., 2018).  
220 A 96-hour time length was considered representative for long-range transport to the receptor site  
221 and to better control the uncertainty of back-trajectories. Sensitivity tests with a 6-day time  
222 length were also performed; however, their results indicate a reduced number of clusters with  
223 lower significant differences in atmospheric parameters and constituents, suggesting that these  
224 longer trajectories may lose part of their specific features.

225 The first issue faced in the calculation of the back-trajectories was the choice of the  
226 meteorological fields used as input, linked to the strongest source of errors (Stohl et al., 2001)  
227 when calculating back-trajectories, and eventually influencing the outcome of the trajectory  
228 clustering (Cabello et al., 2008a).

229 As previously observed in Brattich et al. (2017a, b), the coarse resolution of the terrain model  
230 included in the meteorological databases is generally not able to adequately resolve the  
231 topography of Mt. Cimone. In this work we used the National Center for Environmental  
232 Prediction (NCEP)/National Center for Atmospheric Research (NCAR) reanalysis with a 2.5°  
233 latitude-longitude resolution, 17 pressure levels from 1000 to 10 hPa, and 6 hourly data, which  
234 was the best compromise available at the time we started the back-trajectories calculation. Such a  
235 coarse resolution, too large to resolve mesoscale subsynoptic processes, is still acceptable for our  
236 study since we are most interested in the large-scale flow pattern more meaningful in a long-term  
237 quasi-climatological approach. The vertical motion of the air parcels was calculated from the  
238 vertical velocity fields. As a rule and due to the methodology applied to compute the back-  
239 trajectories (the computation uses the horizontal gradient of the field, calculated as a “centered  
240 difference” with meteorological data on a subgrid that follows the trajectory), it is recommended  
241 that trajectories at three heights are calculated simultaneously (see  
242 <https://www.arl.noaa.gov/hysplit/hysplit-frequently-asked-questions-faqs/faq-hg23/>). In this  
243 case, trajectories were calculated at 2200 m asl (just above the monitoring site), at 3000 m asl  
244 (800 m higher, at the edge of the free troposphere) and at 1400 m asl (above the terrain’s height  
245 for the measurement site in the model, to better consider meteorology below the study site). In  
246 the following, results are reported and discussed only for the height corresponding to that of the  
247 receptor site. The analysis at 3000 m, useful to compare the study site with the free troposphere,  
248 is included in Supporting Information (SI).

249 As for the association between trajectories and samples, each aerosol sample with its  
250 physico-chemical properties was associated with a specific advection pattern only if at least 60%  
251 of the calculated trajectories ending at the site during the sampling corresponded to that  
252 advection pattern. However, samples out of the outlined conditions were also analysed in depth  
253 with emphasis on flows characterized by fast and high-frequency variability often associated  
254 with singular though relevant trajectories (i.e. cutoff lows or Saharan dust incursions).

255 Clusters of back-trajectories were calculated following a clustering procedure based on  
256 the k-means algorithm, with specific features like the use of great-circle distances and  
257 determination of the number of clusters from the evaluation of the classification into k clusters  
258 (considering a large number of replicates), with k running from 15 to 3, (see for example Cabello  
259 et al. (2008b), Dueñas et al. (2011), Perrone et al. (2013), Brattich et al. (2016)). Significant  
260 differences in the analysed meteorological and atmospheric parameters according to the  
261 identified clusters were analysed using the Kruskal-Wallis test, without any “a priori”  
262 assumption of their distribution (Brankov et al., 1998). Whenever significant differences among  
263 the groups were found, pairwise Mann-Whitney tests were performed to identify the significantly  
264 different pairs. Conservatively, p-values in the latter were compared against adjusted  
265 significance levels  $\alpha$  using the Dunn-Sidak correction for multiple comparisons  $\alpha = 1 -$   
266  $(1 - \alpha_t)^{1/n}$ , where  $n = k(k - 1)/2$  is the number of pair-wise comparisons done between k  
267 categories, with overall significance  $\alpha_t = 0.05$ .

268 Composite synoptic charts of 700, 850 and 1000 hPa geopotential height, computed with  
269 data from NCEP/NCAR re-analysis project database (Kalnay et al., 1996), available from the  
270 Earth System Research Laboratory, Physical Sciences Division, of the USA National Oceanic  
271 and Atmospheric Administration (NOAA) at <http://www.esrl.noaa.gov/psd/> were used to analyse  
272 the meteorology of individual situations.

273 The presence of trends in the monthly time series over the study period considered in this  
274 work was examined through a number of nonparametric statistical methods, mainly based on the  
275 Mann-Kendall (M-K) tau test to assess the significance of monotonic trends and the Theil-Sen  
276 (T-S) slope estimate for trend magnitude. In particular, considering that the significance of a  
277 trend is affected by the presence of serial correlation, and, conversely, the estimate of the serial  
278 correlation is also altered by the presence of a trend, the correlation coefficients at different lags  
279 were first estimated by computing the sample autocorrelation function (ACF) for each time  
280 series. The results indicated that, in general, the analysed time series present some degree of  
281 serial correlation, together with seasonality; as a consequence, two methods of trend analysis  
282 have been used with the aim of removing, or reducing, the influence of seasonality and lag-1  
283 autocorrelation in the monthly data:

284 (1) The seasonal Kendall test (Hirsch et al., 1982), which applies the M-K trend test  
285 separately for each month and then combines the results. (2) The trend-free pre-whitening  
286 (TFPW) procedure (Yue et al., 2002) applied to the seasonally adjusted monthly time series, to  
287 remove the influence of the month-to-month correlations in the significance of the trends. The  
288 TFPW procedure comprises several steps, including the linear detrending of the time series using  
289 the T-S slope, the removal of the serial autocorrelation of the residuals and the add-back of the  
290 discarded linear trend to the remaining time series, before the M-K test is applied. Seasonal-trend  
291 decomposition of the time series was used to obtain the de-seasonalized time series, which were  
292 subsequently analysed by the TFPW procedure. The decomposition technique used in this work  
293 (STL decomposition hereafter) is based on LOESS (locally weighted low-degree polynomial  
294 regression), a nonparametric regression technique recursively applied to the seasonal and trend

295 components (Cleveland et al., 1990). Additionally, the resulting (nonlinear) trend component has  
 296 been used for the visual assessment of the long-term behaviour of the time series.

297 The association between the frequency of each advection pattern and observations at the  
 298 sampling site, as well as with the NAOi and other large- and regional-scale teleconnections, has  
 299 been examined for the de-trended monthly time series and for the seasonal means via least-  
 300 square regression analysis with statistical significance evaluated by a two-tailed *t*-test. Since  
 301 relationships are not necessarily linear, the nonparametric Kendall rank test has also been used to  
 302 identify any statistically significant association without any “a priori” assumption of their form.  
 303 Spearman correlation coefficients have been computed for the cases with significant association.

### 304 **3 Results and discussion**

#### 305 **3.1 Characteristics of the main advection pathways**

306 Figure 1 shows the centroids (representative trajectories) of the 8 clusters obtained at 2200 m asl  
 307 and the relative percentage frequency of each flow pattern over the whole 1998-2011 period,  
 308 together with the mean height evolution over time and the monthly variation of the frequency of  
 309 the air flow pathways reaching the receptor site.

310 Cluster names were chosen based on their region of provenance. Most of the trajectories  
 311 correspond to westerly flows; in particular, westerly trajectories are classified into Northern  
 312 Atlantic (N Atl), North America (N Am), Atlantic (Atl), Western (W), and North-Western  
 313 Europe (NW-Eu) flows, together representing more than 60% of the flows. The remaining  
 314 trajectories are classified into Arctic (A), Eastern (E), and Mediterranean-Africa (Me-Af).

315 As from the mean height evolution over time of the representative trajectories reported in  
 316 Figure 1, the Arctic and North-American trajectories descend from the most elevated heights  
 317 while approaching the site, and eventually rise again and cross over the Alps. North Western-  
 318 Europe and Eastern flows do not considerably change their height during their transport, whereas  
 319 Western, Atlantic and (more specifically) Mediterranean-Africa trajectories generally reach the  
 320 observatory from very low levels.

321 Figure 2 shows the box plots of meteorological parameters, i.e., pressure, temperature,  
 322 relative humidity, precipitation, tropopause height, wind speed, and mixing height by advection  
 323 pattern. Similar to Figure 2, Figure 3 depicts box plots for the atmospheric species, such as O<sub>3</sub>,  
 324 CO<sub>2</sub>, BC, CO, fine and coarse particles, PM<sub>10</sub>, <sup>7</sup>Be, and <sup>210</sup>Pb, associated with each flow pattern  
 325 at 2200 m and at 3000 m asl. Additionally, the analysis extends over nuclidic and mass ratios  
 326 such as <sup>7</sup>Be/<sup>210</sup>Pb, <sup>7</sup>Be/PM<sub>10</sub>, <sup>210</sup>Pb/PM<sub>10</sub>, used to gain insights into the vertical motions of air  
 327 masses as well as on convective activity in the troposphere (e.g., Koch et al., 1996), are also  
 328 analysed. The summary statistics together with significant differences of each variable by  
 329 advection pattern is reported in the SI. In order to better characterize the flow pathways, both  
 330 boxplots and summary statistics refer to the “pure cases”, i.e., the samples attributed to only one  
 331 advection pathway (when at least 60% of the trajectories ending at Mt. Cimone during one single  
 332 sampling period belong to the same advection pathway).

333 Below we summarize the major characteristics of the identified advection pathways in  
 334 terms of seasonal variability, mean height, meteorological variables and atmospheric  
 335 composition, as indicated in Figures 2 and 3.

- 336 • A: advection of fast and elevated (mean height of the cluster equal to 3113 m) air masses  
 337 originating in the Arctic/polar regions. This trajectory type is more frequent in autumn  
 338 and winter. This subsiding air flow is associated with low temperatures, low relative  
 339 humidity, low wind speeds, relatively low values of the tropopause height (probably due

340 to the fact that these air masses are not vertically thick compared to other air masses), and  
341 moderate mixing heights. Such air masses can be linked to the presence of lows or cut-off  
342 lows characterized by low tropopause or tropopause folding and in fact are also  
343 associated with rather low pressure systems. Due to their subsiding nature, travelling at  
344 high altitudes over remote regions, these air masses are generally moderately clean, i.e.  
345 associated with low values of O<sub>3</sub>, black carbon, CO, PM<sub>10</sub>, and <sup>210</sup>Pb. It is also associated  
346 with high <sup>7</sup>Be and therefore with high <sup>7</sup>Be/<sup>210</sup>Pb and <sup>7</sup>Be/PM<sub>10</sub>. This kind of transport is  
347 in fact frequently associated with STE, in agreement with previous observations of  
348 stratospheric intrusions at Mt Cimone (Bonasoni et al., 1999, 2000a, 2000b; Brattich et  
349 al., 2017a). In particular, the high <sup>7</sup>Be, <sup>7</sup>Be/<sup>210</sup>Pb and <sup>7</sup>Be/PM<sub>10</sub> can be attributed to the  
350 high production rate of <sup>7</sup>Be in the stratospheric air at high latitudes (Beer et al., 2012), ,  
351 even though the reduced ozone concentration points out a connection with subsidence  
352 from the upper troposphere, a region connected with increases in <sup>7</sup>Be but not in O<sub>3</sub>.

- 353 • E: advection of relatively slow and low (mean height equal to 2190 m) air masses from  
354 East. This flow type is more frequent in April, May and September, and groups the 13%  
355 of the trajectories. These air flows are associated with low tropopause height, while  
356 pressure, wind speeds, humidity, and mixing height take intermediate values. This flow  
357 type brings lower concentrations of PM<sub>10</sub> than the Western advection, but is associated  
358 with higher loadings of fine than coarse particles, in agreement with observations by  
359 Tositti et al. (2013). This flow type is also associated with moderately high black carbon  
360 and high <sup>210</sup>Pb, and to the lowest values of <sup>7</sup>Be/<sup>210</sup>Pb activity ratio; overall this flow can  
361 be labelled as “continental polluted”.
- 362 • Me-Af: relatively short and low (mean height equal to 2154 m) Mediterranean and North-  
363 African air masses. These trajectories, grouping the 18% of the total, are active all-year  
364 round but mainly in spring and autumn. These flows cross over the Mediterranean at low  
365 altitude and correspondingly are warm and humid, and are associated with low wind  
366 speeds and intermediate mixing height (close to 1400 m, which is below the typical mean  
367 height reported for Saharan dust transport, between 1500 and 4000 m asl; see Jorba et al.,  
368 2004 and Papayannis et al., 2008). These air masses bring substantial PM<sub>10</sub> loadings as  
369 linked to Saharan Dust transport (in agreement with Duchi et al., 2016), associated with  
370 increases in both fine and coarse sized particles. It contributes also to BC and to high  
371 <sup>210</sup>Pb and <sup>7</sup>Be concentrations, and thus to rather low <sup>7</sup>Be/<sup>210</sup>Pb, <sup>7</sup>Be/PM<sub>10</sub> and <sup>210</sup>Pb/PM<sub>10</sub>  
372 ratios. Overall, this flow may be labelled as “African convective”, including the often-  
373 observed biomass burning tracers. In particular, similar to what Dueñas et al. (2011) and  
374 Brattich et al. (2017a) reported, Mediterranean-Africa air masses are linked to high  
375 activities of both <sup>7</sup>Be and <sup>210</sup>Pb, due to the combination of downward transport from the  
376 upper troposphere and African dust uplifting.
- 377 • W: advection of relatively slow and low-level (mean height equal to 1915 m) air masses  
378 from West, which are active all year round but are more frequent in July, August, and  
379 October. This flow pattern groups the 15% of the trajectories. These air masses are  
380 associated with high pressures, high temperatures, low relative humidity, high tropopause  
381 height, moderate wind speeds, and moderate-to-high mixing heights. This advection  
382 pattern carries elevated values of O<sub>3</sub>, PM<sub>10</sub>, fine and coarse particles; it contributes to a  
383 large degree also to black carbon, a tracer of combustion. This is likely related to of the  
384 entrainment of aged, polluted air masses into this flow type when crossing coastal areas  
385 in the western Mediterranean. It contributes also to high <sup>210</sup>Pb and <sup>7</sup>Be concentrations

- 386 (low  ${}^7\text{Be}/\text{PM}_{10}$ ,  ${}^{210}\text{Pb}/\text{PM}_{10}$  and  ${}^7\text{Be}/{}^{210}\text{Pb}$  ratios) suggesting associated convective  
 387 pathways.
- 388 • Atl: relatively fast and low-level (mean height equal to 1974 m) air masses coming from  
 389 the Atlantic Ocean. This advection pattern is most common from October to April. It  
 390 groups only the 8% of the trajectories. These air masses are moderately warm and humid,  
 391 present low pressure levels, moderate to high wind speeds, and low mixing heights. This  
 392 advection pattern shows low contributions of  $\text{O}_3$ , black carbon,  $\text{PM}_{10}$ ,  ${}^7\text{Be}$  and  ${}^{210}\text{Pb}$ , as a  
 393 consequence of the renewal of air masses by these strong mid latitude maritime flows and  
 394 the relatively high wind speeds recorded at the site.
  - 395 • N-Am: polar fast and upper level (mean height of the cluster equal to 2965 m) air masses  
 396 that originate as continental air over North America. This air mass type is negligible in  
 397 summer months, mostly occurring from October to April. This advection pattern is the  
 398 least frequent among those emerged for Mt. Cimone (5% of the trajectories arriving at the  
 399 receptor site). Similar to the Arctic type, these are cold, dry subsiding flows. They are  
 400 related to the lowest temperatures (even lower than the Arctic ones), lowest pressure  
 401 levels, low relative humidity, low tropopause heights and mixing heights, and moderate  
 402 wind speeds at the study site. The polar-front jet stream is present at upper levels. North  
 403 American air masses are usually very clean (low in  $\text{O}_3$ , black carbon,  $\text{CO}$ ,  $\text{PM}_{10}$  as well  
 404 as in both fine and coarse particles), with the lowest mean and median values of these  
 405 species. The cleanliness of these flows derives from their subsiding nature originating  
 406 quite high above the North American region, and reaching Mt. Cimone (i.e. southern  
 407 Europe) at moderately high wind speeds. This results in the replacement of air masses  
 408 with cleaner, fresh air, as previously observed also at other southern Mediterranean sites  
 409 in Spain and Italy (e.g., Cabello et al., 2008b; Perrone et al., 2013, 2014). Also the  
 410 atmospheric radiotracers  ${}^7\text{Be}$  and  ${}^{210}\text{Pb}$  present low concentrations within this flow type,  
 411 probably due to the low concentration of suspended fine particles and relatively younger  
 412 upper level air masses.
  - 413 • N-Atl: relatively fast, but not very high (mean height of the cluster equal to 2562 m) air  
 414 masses coming from the Northern-Atlantic Ocean. Active throughout the year with  
 415 highest frequency in July. This group of trajectories comprehends the 14% of the total.  
 416 These air masses are moderately warm, very humid, and connected to slow wind speeds  
 417 and high mixing height. This flow pattern shows elevated contributions of  $\text{O}_3$  and fine  
 418 particles, but low values of black carbon, carbon monoxide and  ${}^{210}\text{Pb}$ , while it  
 419 contributes moderately to  $\text{PM}_{10}$  and  ${}^7\text{Be}$  (low  ${}^7\text{Be}/\text{PM}_{10}$ ,  ${}^{210}\text{Pb}/\text{PM}_{10}$  and  ${}^7\text{Be}/{}^{210}\text{Pb}$  ratios),  
 420 probably due to contribution of aged pollutants from Western Europe where they travel  
 421 after their residence over the North-Atlantic Ocean, in agreement with Brattich et al.  
 422 (2016).
  - 423 • NW-Eu: slow and not very high (mean height equal to 2321 m) continental air masses  
 424 coming from North Western-Europe. This flow pattern, with mean height equal to 2321  
 425 m, is more frequent in summer months and groups the 19% of the trajectories. These air  
 426 flows present the lowest wind speeds and high pressures, frequently related to blocking  
 427 situations in the summertime; they are also related to high temperatures, relative humidity  
 428 and mixing height. Similar to the Eastern advection, it brings lower concentrations of  
 429 particulate matter with respect to the Western flow type, but associated with higher  
 430 loadings of fine particles than coarse ones. These flows contribute moderately, together

431 with Eastern air masses, to black carbon and to high  $^{210}\text{Pb}$  (low  $^7\text{Be}/\text{PM}_{10}$ ,  $^{210}\text{Pb}/\text{PM}_{10}$  and  
432  $^7\text{Be}/^{210}\text{Pb}$  ratios).  
433

### 434 3.2 Atmospheric parameters by advection pattern

435 The large-scale advection pathways found at Mt. Cimone have been described in terms of  
436 meteorological variables and atmospheric composition in the previous subsection. Summarizing,  
437 North Atlantic and NW Europe advections, both passing over the British Isles and France,  
438 present the highest  $\text{O}_3$  levels. In turn, Atlantic as well as North America and Arctic air flows are  
439 associated with low  $\text{O}_3$  values, which points out the influence of precursor levels.  $\text{CO}_2$ , a long-  
440 lived greenhouse gas, is well-mixed in the free troposphere and not much affected by the  
441 boundary layer dynamics, with values homogeneously distributed over all the flow types. While  
442 Mediterranean Africa and Western air masses are associated with high number of both fine and  
443 coarse particles, as related to the transport of marine and desert particles together with  
444 anthropogenic pollution, North Atlantic advections are high only in fine particles related to the  
445 transport of polluted particles from anthropogenic origin.

446 Low values of the  $^{210}\text{Pb}$  crustal tracer are observed when air masses arrive from the ocean  
447 (Atlantic, North Atlantic and Northern America) as expected, while  $^{210}\text{Pb}$  maxima are linked to  
448 flows with an explicit continental origin such as Mediterranean-Africa, Western, Eastern and  
449 North Western-Europe. This behaviour is of course due to  $^{210}\text{Pb}$  continental origin, as  $^{222}\text{Rn}$  flux  
450 from the oceans into the atmosphere is negligible due to its low marine source (low radon  
451 emission) (Balkanski et al., 1993; Baskaran, 2011).  $^7\text{Be}$  low values are connected to Atlantic and  
452 Northern American air masses, while Western flows are related to the highest values, likely  
453 connected to Gulf of Genoa and Gulf of Lion cyclogenesis, which have been long recognized as  
454 associated with STE (e.g., Stohl et al., 2000; Aebischer and Schär, 1998).

455 Here it is worth noting that due to the coarse resolution of the meteorological field we are  
456 using, our methodology is not able to resolve mesoscale and subsynoptic processes. However,  
457 such processes may have important effects on the variability of the atmospheric species we are  
458 considering. In particular, some of the identified advection pathways (the local and regional  
459 transports) can be associated with favourable “stagnation” conditions (mostly during the summer  
460 months), such as the increase in height of the regional PBL and/or mountain/valley breeze  
461 regimes, as previously investigated by Cristofanelli et al. (2013, 2016).

462 Figures 4 and 5 analyse the connection of the seasonality of advection pathways with that  
463 of radiotracers and  $\text{PM}_{10}$ , respectively. The seasonality of variables was analysed considering  
464 monthly medians as the distributions of  $\text{PM}_{10}$  and of atmospheric radiotracers are decidedly non-  
465 Gaussian (Tositti et al., 2013, 2014), and in this case the median should be preferred over the  
466 arithmetic mean as a more robust indicator (e.g., Wilks, 2011).

467 As shown in Figure 4 and as previously highlighted (Tositti et al., 2014; Brattich et al.,  
468 2016, 2017a), the seasonal behaviour of  $^{210}\text{Pb}$  is characterized by the presence of one summer  
469 maximum mainly due to higher mixing height and enhanced uplift from the boundary layer.  
470 Conversely,  $^7\text{Be}$  seasonal variations are more complex, being characterized by two relative  
471 maxima, one during the cold season (March) associated with an increased frequency of STE  
472 (James et al., 2003; Stohl et al., 2003; Brattich et al., 2017a) and one in the warm season mainly  
473 (but not exclusively) associated with tropospheric subsidence balancing low tropospheric air  
474 masses uplift generated by the convective circulation produced by the intense solar heating and  
475 the higher tropopause height increase of this season (Ioannidou et al., 2014), occasionally  
476 accompanied by STE (Cristofanelli et al., 2009a; Tositti et al., 2014). Figure 5 highlights,

477 however, that the seasonality of radionuclides can also be connected to the seasonality of air  
478 mass transport at the site, as previously pointed out by Brattich et al. (2017b) by means of model  
479 simulations with a Chemistry and Transport Model. In fact, while  $^7\text{Be}$  March maximum seems to  
480 be related to the seasonal pattern of Arctic air masses (as Atlantic and North American air  
481 masses, presenting also a simultaneous winter peak, are associated with lower  $^7\text{Be}$  values in the  
482 boxplots of Figure 3), the  $^7\text{Be}$  summer maximum seems to correspond to that presented by  
483 Mediterranean-Africa, Western and North Atlantic air masses.  $^{210}\text{Pb}$  summer maximum seems  
484 instead to be well related with the seasonality of Western and North Western-Europe flows.  
485 However the monthly analysis is not capable of resolving the contributions of advection  
486 pathways occurring in the same month and therefore to uniquely determine a clear connection  
487 between advection pattern and concentration.

488 Figure 5 provides similar analyses for the  $\text{PM}_{10}$  seasonal pattern, which, like  $^{210}\text{Pb}$ , show  
489 minimum values during the cold season and maxima during summer months, when it is uplifted  
490 from the regional boundary layer due to thermal convection and increased mixing height (Tositti  
491 et al., 2013). The seasonal pattern of  $\text{PM}_{10}$  might be, however, influenced by the seasonal pattern  
492 of advection pathways bringing about elevated mass loads of particles, such as Mediterranean-  
493 Africa, Western, North Atlantic and North Western-Europe air masses. In particular, while the  
494 seasonal maximum frequency of Mediterranean-Africa in June contributes to the first  $\text{PM}_{10}$   
495 increase observed during this month, July values are related to the contribution of North Atlantic  
496 flows, and August elevated values are linked to the seasonal pattern of Western and North  
497 Western-Europe advections. Figure 6 also shows that the magnitude of the peaks is determined  
498 by both the source of trajectories and the concentration over source regions, as indicated by the  
499 analysis of the time spent by trajectories over North Africa together with the aerosol optical  
500 depth (AOD) over Africa from MODIS Aqua 5.1 collection (Deep Blue AOD at 550 nm). We  
501 have found that trajectories spend more time over northern Africa in November than in May, but  
502 AOD in Africa is lower in November (mean equal to 0.125 in November vs. 0.396 in May), an  
503 observation consistent with the low  $\text{PM}_{10}$  concentration in November. Similarly, the AOD at 550  
504 nm (Land and Ocean) along the western Mediterranean shows higher values for May than for  
505 November (0.27 vs. 0.14).

506 Though the seasonal frequency of events accounts for most of the variability, a detailed  
507 analysis shows that singular events may make important contributions to some of the parameters  
508 observed. For this reason, Figure 6 reports boxplots of the median  $^7\text{Be}/^{210}\text{Pb}$  contribution per  
509 number of episodes for each season. Figure 8 highlights that both summer Arctic as well as  
510 summer North-American flows, though being infrequent, can contribute to increases in  $^7\text{Be}$  (and  
511 not in  $^{210}\text{Pb}$ ). Their average contribution to high  $^7\text{Be}/^{210}\text{Pb}$  during summertime is higher than  
512 during winter when they are more frequent. Figure 8 also emphasizes Arctic, North Atlantic,  
513 North-American and Western flows as the main contributors to winter  $^7\text{Be}/^{210}\text{Pb}$  increases;  
514 Mediterranean-Africa flows are instead associated with expectedly large contributions of  $^{210}\text{Pb}$   
515 and  $\text{PM}_{10}$ , while less obvious, but in agreement with previous studies (Hernández et al., 2008;  
516 Menut et al., 2009; Dueñas et al., 2011; Gordo et al., 2015), is the inherently high contribution in  
517  $^7\text{Be}$ . The high  $^7\text{Be}$  of this flow type can be connected to the intense convection generated by the  
518 extremely high temperature of the ground and the very dry conditions in the Sahara desert  
519 together with the mineral dust size spectrum including also a large fraction of submicron  
520 particles to which  $^7\text{Be}$  attaches (Brattich et al., 2017a). This confirms how, given the suitable  
521 dynamical framework, the  $^7\text{Be}/^{210}\text{Pb}$  ratio is a pragmatic and efficient proxy of vertical motion.

522

523 **3.3 Trend analysis of transport pathways, teleconnection indices and atmospheric composition**

524 The assessment of the existence of temporal trends in the time series of the monthly frequencies  
525 of the air flow types, as well as of monthly medians of the variables and of teleconnection  
526 indices has considered the presence of seasonality and serial correlations in the time series (see  
527 SI). Indeed, as previously reported in the Methodology section, the analysis of the pattern of the  
528 ACF (AutoCorrelation Function) can reveal the presence of seasonality in the time series. Here,  
529 the previously described seasonal nature of the advection pathways, as well as of the analysed  
530 atmospheric variables, is also evidenced by the periodic behaviour of the ACF of their monthly  
531 frequencies of occurrence (in the case of advection types) and monthly medians (in the case of  
532 atmospheric species), with maxima and minima beyond bounds of significance (95% confidence)  
533 and a full cycle of 12 months. Examples of ACF are reported in the SI. In all cases the use of the  
534 STL (Seasonal and Trend decomposition using Loess) decomposition allowed the estimation of  
535 the relative contributions of the seasonal, trend and residual components, and the subsequent  
536 removal of the periodic structure (connected with the seasonal component) in the ACF for further  
537 analysis.

538 Since significant data loss occurred for technical reasons in 2007, the trend analysis was  
539 restricted only to the 1999-2006 time window. Although this time period is too short to provide  
540 definitive trend assessment, this analysis can provide useful hints as to the role of specific  
541 processes (e.g. meteorology vs anthropogenic emissions vs atmospheric transport) in modulating  
542 the variability of the atmospheric species. In addition, considering the decreasing number of  
543 samples towards the end of the time series and the consequent decrease in the number of  
544 trajectories, for the analysis of trends we considered the corresponding fraction of each trajectory  
545 type with respect to the total number of trajectories in a month. At this step of the research we  
546 also included in the analysis the tropopause height data obtained from the Aqua AIRS  
547 satellite, available since August 2002 from the NASA Goddard Earth Sciences Data and  
548 Information Services Center (<http://mirador.gsfc.nasa.gov/>). The comparison of the tropopause  
549 height from radiosoundings and from satellite observations yields a strong significant correlation  
550 ( $R^2 = 0.83$  for the monthly means and  $R^2 = 0.71$  for the monthly medians).

551 Trend analysis on air flow pathways reveals some significant tendencies though of  
552 limited extent and also with some differences according to the different approaches applied, in  
553 particular seasonal Kendall test and trend-free pre-whitening methods (see Table 2). Both  
554 methods consistently detect significant trends in a number of cases, in particular indicating an  
555 increasing trend for Arctic flows and a decreasing one for Western flows. The seasonal absence  
556 of both Arctic and North-American flows strongly biases the Theil-Sen slope to zero. However,  
557 the seasonal Kendall tests suggest the presence of a significant trend in the Arctic time series,  
558 and deseasonalization provides a better estimate of the upward trend. As for the variables, the  
559 results indicate a strong upward trend for CO<sub>2</sub>, in agreement with the long-term CO<sub>2</sub> behaviour at  
560 the global scale (Machta, 1972; Thoning et al., 1989; Randerson et al., 1997; WMO-GAW,  
561 2017), and a significant decreasing trend for both the monthly medians of <sup>210</sup>Pb and PM<sub>10</sub>  
562 measured at the station in the period 1999-2006 (Figure 7). The mean annual change of the  
563 original monthly time series is equal to +1.80 ppm year<sup>-1</sup>, -0.008 mBq m<sup>-3</sup> year<sup>-1</sup> and -0.15 μg m<sup>-3</sup>  
564 year<sup>-1</sup>, for CO<sub>2</sub>, <sup>210</sup>Pb and PM<sub>10</sub> respectively, while for the de-seasonalized monthly series it is  
565 equal to +1.90 ppm year<sup>-1</sup>, -0.01 mBq m<sup>-3</sup> year<sup>-1</sup> and -0.30 μg m<sup>-3</sup> year<sup>-1</sup>.

566 The detection of contemporary decreasing trends of <sup>210</sup>Pb and PM<sub>10</sub> is particularly  
567 important in light of the decreasing trend of PM<sub>10</sub> in the period late 90's-2010 observed in many  
568 stations in Europe, especially at regional background stations (Pérez et al., 2008; Barmpadimos  
569 et al., 2011; Colette et al., 2011; Barmpadimos et al., 2012). Generally, this PM<sub>10</sub> drop is

570 attributed both to a decrease in anthropogenic emissions, as a result of to the mitigation strategies  
571 adopted, as well as to different meteorological processes or cycles, such as the frequency and  
572 intensity of Saharan dust episodes (Pérez et al., 2008). Both Colette et al. (2011) and  
573 Barmpadimos et al. (2012) showed that the decrease in anthropogenic emissions seems to be  
574 more important than meteorology as a driving factor for the observed decrease. However, in our  
575 case the observation of a contemporary decreasing trend of the  $^{210}\text{Pb}$  radionuclide at this remote  
576 background site, which cannot be ascribed to a decrease in anthropogenic emissions due to the  
577 crustal natural origin of this nuclide, highlights the important role played by meteorology in  
578 these decreases.

579 A visual inspection of the time series and their trend components obtained from the  
580 seasonal-trend decomposition analysis (Figure 7) suggests that the upward trend of Arctic flows  
581 was significant from 2002 on, while Western flows downward trend was almost constant over  
582 the 1999-2006 study period. While  $\text{CO}_2$  presents an upward trend over the time period, in  
583 agreement with, e.g., WMO-GAW global analyses (2017), for  $^{210}\text{Pb}$  and  $\text{PM}_{10}$  the decreasing  
584 trend is stronger after 2001. Besides parameters characterised by the existence of significant  
585 trends, we also reported results for the two NAO indices with the aim of illustrating the result for  
586 this well-known and often studied teleconnection index, showing a slightly decreasing non-  
587 significant trend.

588 The increase in  $^{210}\text{Pb}$  activity from 2002 to 2003 might be due to the extremely high  
589 temperature recorded in the whole European region, especially during the summer months  
590 (Cristofanelli et al., 2009a; Pace et al., 2005), and connected also to anomalously high ozone  
591 concentrations at Mt. Cimone (Cristofanelli et al., 2007) and to augmented radon exhalation  
592 during the 2003 summer heat wave in Europe. In  $\text{PM}_{10}$  this increase is masked by the 2004  
593 maximum connected to an exceptional Saharan dust episode previously described (Beine et al.,  
594 2005) which resulted in an event concentration reaching  $80 \mu\text{g m}^{-3}$  and characterized by a  
595 significant increase in the coarse fraction and a reduced, though not negligible, increase in the  
596 fine fraction (to which radionuclides attach), and with a less substantial increase in  $^{210}\text{Pb}$  than in  
597  $\text{PM}_{10}$  (Tositti et al., 2013; Brattich et al., 2015a, b).

598 The analysis of the two tropopause height datasets shows no trends at Mt. Cimone,  
599 contrarily to the increasing trend observed globally and suggested as an alternative detection  
600 variable of climate change (e.g., Añel et al., 2006), connected to the increase in atmospheric  $\text{CO}_2$   
601 leading to tropospheric warming and stratospheric cooling, and to anthropogenically induced  
602 depletion of stratospheric ozone, also inducing stratospheric cooling (e.g., see Chapter 5 of  
603 WMO, 2007; Myhre et al., 2013; Santer et al., 2013). The absence of trends in our case is  
604 possibly due to the different and short time window we use.

605 Both of the NAOi time series (the station-based and the Principal Components-based) do  
606 not show any significant trends according to the tests, despite presenting a negative T-S slope.  
607 For the sake of completeness, we also investigated the results for the CRU station-based NAOi  
608 which indicate the absence of statistically significant trends during the analysed period. The only  
609 teleconnection index presenting a significant trend during the study period is the WeMOi, with a  
610 downward trend constant over the study period. The downward trend is particularly evident in  
611 2005 and 2006 in correspondence with very large negative indices indicative of the presence of  
612 strong lows in the Gulf of Cádiz and anticyclones in central Europe and associated with an  
613 increase of humid airflows travelling over the Mediterranean Sea and a reduction of westerly-  
614 northwesterly flows.

615 The analysis of the magnitude of the seasonal and trend components of the time series  
 616 revealed that the seasonal component dominates over the trend component and the small-time  
 617 scale variations in almost all the measured atmospheric variables, weighting about twice the  
 618 trend component. In turn, the small-scale variations dominate most of the teleconnection indices  
 619 with the exception of MOi, and the frequencies of the different advection pathways.

### 621 **3.4 Association among air flow types, meteorological/atmospheric parameters and teleconnection** 622 **indices**

623 In this work, the degree of association among air flow types, meteorological/atmospheric  
 624 parameters and teleconnection indices is assessed by analyzing the Spearman correlation  
 625 coefficient, considering both the complete yearly time series and separately by season.

626 Figure 8 shows the linear Spearman correlation coefficients between teleconnection  
 627 indices and flow types, while comprehensive tables with all the correlation coefficients are  
 628 reported in the SI.

629 The NAO is related to North-American flows (especially in winter), and weakly related  
 630 to Mediterranean-Africa (during summer and all-yearlong) and North-Atlantic pathways. It is  
 631 recognized that the positive NAO phase corresponding to a stronger than usual subtropical high-  
 632 pressure centre and deeper than normal Icelandic low results in more and stronger winter storms  
 633 crossing the Atlantic Ocean on a more northerly track, while the negative phase is connected to  
 634 fewer and weaker winter storms crossing on a more west-east pathway (Barnston and Livezey,  
 635 1987). An anti-correlation of westerly flows reaching three Mediterranean sites (Lecce, Elche  
 636 and Malaga) with NAOi was previously observed by Orza et al. (2013): this observation is  
 637 connected with the fact that the position of the subtropical high at lower latitudes during the  
 638 negative phase of the NAO promotes the access of westerlies (W)/southwesterlies (Me-AF) to  
 639 the Mediterranean. This is shown in Figure 9, presenting for each spatial grid cell the ratio  
 640 between the residence time of the air parcels reaching Mt. Cimone during the positive and the  
 641 negative phases of NAO (NAOi higher than +0.5 and lower than -0.5, respectively) for the  
 642 extended winter period (DJFM), calculated as the number of trajectory endpoints falling within  
 643 each area of interest divided by the total number of trajectory endpoints for the entire set of  
 644 trajectories in the considered time period.

645 Figure 9 reveals that south-westerlies and slower westerlies from the westernmost part of  
 646 Northern Africa and southern Spain are more frequent during the negative phase of the NAO,  
 647 while flows from Libya and surrounding regions (also belonging to the Mediterranean-Africa  
 648 cluster) occur preferentially during the positive NAO phase. Moreover, trajectories coming from  
 649 North-America are more frequent during the positive phase of NAO, as indicated by the  
 650 significant high correlation between North-American flows and NAO. Finally, North-Eastern  
 651 flows seem to be more usually observed during the positive NAO phase, even if this was not  
 652 readily observed from the correlation analysis.

653 The frequencies of Atlantic, North-Atlantic, North-American and Western flows are  
 654 related to the WeMOi. In particular, while Atlantic, North-American and Western flows are  
 655 related to the WeMOi both all-yearlong and during separate seasons specific for each advection  
 656 pattern, the frequency of North-Atlantic trajectories is strongly connected with WeMOi in  
 657 summer, and less so considering the whole time series. It is also weakly negatively related to the  
 658 Eastern advection pattern. These correlations can be easily understood considering that this index  
 659 measures the difference between the standardized surface pressure values measured in Padua

660 (Italy), and San Fernando (Cadiz, Spain). Therefore, these results suggest a likely connection of  
661 the downward trends of Western flows with WeMOi as previously observed.

662 MOi presents weak relations with Western and North-Western Europe pathways, and  
663 with North-American flows during winter. Also these relations can be easily understood from the  
664 MOi construction as the difference of standardised geopotential height anomalies at Algiers  
665 (Alger) and Cairo (Egypt).

666 EA, consisting of a north-south dipole of anomaly centres displaced South-Eastern with  
667 respect to the NAO ones, appears negatively related to Arctic flows (especially in autumn, and  
668 secondarily in winter and all-yearlong), and positively associated with Western (mostly in  
669 winter) and Atlantic flows (not in spring). Its relation with Me-AF has only a winter nature.

670 EA/WR and SCA indices present less relations with air mass pathways, probably due to  
671 their limited influence in central Europe; in fact, the EA/WR presents an association with  
672 Western flows only during autumn, while the SCA pattern is negatively correlated with Western,  
673 Atlantic, North-American and North-Atlantic pathways during winter, while positive  
674 associations with North-American and Western flows are observed during summer and autumn,  
675 respectively.

676 Figure 10 similarly reports the correlation coefficients between teleconnection indices  
677 and the monthly medians of and atmospheric composition variables.

678 The positive correlation of NAO during the transition seasons with particles  
679 concentration, even though not statistically significant, is linked to the fact that the positive NAO  
680 phases are associated with drier weather conditions in the Mediterranean area which generate  
681 intense uplift of particles from the ground; on the contrary, the negative correlation between the  
682 station-based NAOi and coarse particles is linked to their transport from Western and  
683 Mediterranean-Africa, and to a lesser extent from North Western-Europe flows, and to the  
684 association of the negative NAO phase with more westerlies/south-westerlies entering the  
685 Mediterranean. The association of the PC-based NAOi to O<sub>3</sub> during summer is in agreement with  
686 the results of Pausata et al. (2012) and is linked to the drier conditions in the Mediterranean area  
687 associated with the positive NAO phase resulting in the build-up of O<sub>3</sub> because of photochemical  
688 processes; however, the transport of O<sub>3</sub> enriched air masses from the Atlantic Ocean, where O<sub>3</sub>  
689 build-up is linked to the low dispersion capacity of precursors, increase of the photochemical  
690 yield and of kinetic reactions due to the high temperature, cannot be completely ruled out. In  
691 particular, Pausata et al. (2012) associated the O<sub>3</sub> increase in south-western Europe to transport  
692 of air masses from continental Europe, favoured by the presence of a more extended Azores  
693 anticyclone. In the case of Mt. Cimone, we observed an increase of Me-AF transport linked with  
694 the positive NAO phase. As such, the positive correlation of O<sub>3</sub> with NAOi could be linked to  
695 the role of mesoscale circulations (enhanced vertical transport and photochemistry under  
696 anticyclonic conditions) which are not resolved in our study due to the coarse resolution of the  
697 meteorological field we are using. The index showing the highest number of significant  
698 correlations with the variables is the MOi (both indices). In the MO positive phase, when higher  
699 pressures are found over the western and central Mediterranean, the storm track is displaced  
700 northward and the orientation of the westerly airflows is modified. This causes dry conditions in  
701 the Mediterranean basin, with low precipitation and relative humidity. Conversely, low pressures  
702 and in particular cyclogenesis over the western/central Mediterranean, which are linked to the  
703 negative MO phase, are associated with precipitation and high <sup>7</sup>Be/<sup>210</sup>Pb and <sup>7</sup>Be/PM<sub>10</sub> ratios.

704 Figure 11 reports the associations between monthly medians of the variables and  
705 frequencies of air flow types during different seasons as well as throughout the year. Most of

706 these associations agrees with Figure 3. Amongst the correlations observed, it appears  
707 particularly important and interesting to discuss those likely to be connected with the  $^{210}\text{Pb}$  and  
708  $\text{PM}_{10}$  negative trends observed in the previous section: Arctic flows, presenting an upward trend,  
709 are negatively related with  $^{210}\text{Pb}$  and  $\text{PM}_{10}$  (all year-long, even though a positive relation during  
710 winter season also appears), while Western flows, presenting a downward trend, are positively  
711 associated with  $^{210}\text{Pb}$  and  $\text{PM}_{10}$ . The anti-correlation of Arctic flows with  $^{210}\text{Pb}$  and  $\text{PM}_{10}$  is  
712 mainly related to the continental origin of  $^{210}\text{Pb}$  and  $\text{PM}_{10}$ , in agreement with Brattich et al.  
713 (2016, 2017b). In the Supplementary Material, tables reporting all significant correlation  
714 coefficients between teleconnection indices/advection pathways and variables are reported.  
715

#### 716 **4 Summary and conclusions**

717 This work focused on finding relationships between the advection pathways and atmospheric  
718 composition observed in a long time series of essential climate variables (ECVs) observed at the  
719 WMO-GAW station of Mt. Cimone (Italy). Advection pathways were identified by a cluster  
720 analysis of back trajectories starting at Mt. Cimone at three different heights; the cluster analysis  
721 identified 8 groups at the initiation height of 2200 m, approximately at the height of the station.  
722 The results reflect strong seasonal pathways with prevalence of westerlies as typical of mid-  
723 latitude Northern Hemisphere sites. The main features of these flow pathways, both from the  
724 meteorological and from the atmospheric composition point of view, were analyzed. The results  
725 indicate that North-American air masses, associated with subsiding flows originating at high  
726 altitudes, are related to low pressures and tropopause heights, cold, and dry air masses, and  
727 linked to high wind speeds. These flows are negligible during summertime, besides being related  
728 to low concentrations of atmospheric pollutants such as BC, CO, O<sub>3</sub>,  $\text{PM}_{10}$ , but also of  
729 atmospheric radionuclides  $^7\text{Be}$  and  $^{210}\text{Pb}$ . Arctic flows are typically cold (though less than North  
730 American ones) and more frequent in the cold season. Being subsiding flows and travelling at  
731 high altitudes over remote ocean and ice, they are also connected to low values of atmospheric  
732 pollutants such as CO, O<sub>3</sub>, BC, but also of particulate matter and  $^{210}\text{Pb}$ . On the contrary, but for  
733 the same reason, this flow type is associated with high  $^7\text{Be}$  and seems connected to SI events.  
734 Continental flows from North-Western Europe, Eastern Europe, Western and Mediterranean-  
735 Africa are generally linked to higher values of atmospheric components; in particular, NW-  
736 Europe, Western and Eastern flows are related to “pollution” events, being associated with high  
737 levels of CO, BC, O<sub>3</sub> and fine particles number densities, leading to corresponding increases in  
738  $\text{PM}_{10}$ . In those cases, the relatively “short” back-trajectories suggest the occurrence of  
739 meteorological conditions characterised by low ventilation that, especially during warm months,  
740 can also promote the diurnal-scale transport of PBL air-masses to the receptor site (Cristofanelli  
741 et al., 2017). Because of their continental origin, these flows are also associated with high  $^{210}\text{Pb}$   
742 levels. Mediterranean-Africa flows associated with Saharan Dust events bring about high  $\text{PM}_{10}$   
743 values, both in the fine and coarse fraction of particles. Interestingly, this flow type was not only  
744 associated with high  $^{210}\text{Pb}$  values, but also with high  $^7\text{Be}$ , which could be connected to the  
745 combination of African dust uplifting and subsidence from the upper troposphere.

746 The association of the seasonality of air mass transports with the seasonality of  
747 radionuclides and particulate matter has also been studied. In fact, while  $^7\text{Be}$  winter maximum is  
748 related to the seasonal behaviour of Arctic and North-Atlantic air masses that reach Mt. Cimone  
749 after traversing the Alps,  $^7\text{Be}$  summer maximum can be connected to the seasonal pattern of  
750 Mediterranean-Africa, Western and North Atlantic air masses.  $^{210}\text{Pb}$  summer maximum is well

751 related with the seasonality of Western and North Western-Europe flows, whereas the seasonal  
752 pattern of PM<sub>10</sub> might be, however, influenced by the seasonal pattern of advection types  
753 bringing about elevated mass loads of particles, such as Mediterranean-Africa, Western, North  
754 Atlantic and North Western-Europe flows.

755 Temporal trends were detected by means of non-parametric techniques applied on the  
756 monthly frequencies of flow types and on monthly medians: over the period 1999-2006, an  
757 upward trend for Arctic flows and a downward trend for Western flows reaching Mt. Cimone at  
758 2200 m was detected. In addition, a downward trend for the monthly medians of <sup>210</sup>Pb and PM<sub>10</sub>  
759 measured at the station, and a contemporary downward trend for WeMOi during the study  
760 period, possibly connected to the decreasing trend of Western flows, were also detected. The  
761 simultaneous decreasing trends of both <sup>210</sup>Pb and PM<sub>10</sub> cannot be ascribed exclusively to a  
762 decrease in anthropogenic emissions, highlighting the potential influence exerted by  
763 meteorology, and suggesting further investigations. In particular, the observation of a positive  
764 correlation of <sup>210</sup>Pb and PM<sub>10</sub> with Western air masses, showing a decreasing trend, and a negative  
765 correlation with Arctic flows, presenting an increasing trend, seems to largely explain the PM<sub>10</sub> and  
766 <sup>210</sup>Pb trends observed in the time series. Significant upward temporal trends were detected for  
767 CO<sub>2</sub>, in agreement with longer time records. The analysis of the magnitude of the seasonal and  
768 trend components of the monthly time series revealed that the largest variabilities in almost all  
769 the studied atmospheric variables are associated with the seasonal components, with a reduced  
770 weight of the trend component for all the series.

771 The association of teleconnection indices with advection pathways and atmospheric  
772 variables was also examined. In particular, positive associations of NAOi with the frequency of  
773 North-American, Atlantic and North-Atlantic flows, and between WeMOi and Western, Atlantic  
774 North-American and North-Atlantic flow types, were observed. The relationship between  
775 teleconnection indices and atmospheric variables highlight the significant influence of regional  
776 short scale modes of variability, like MO, over synoptic conditions and atmospheric conditions at  
777 the sampling site.

778 The results of this work highlight the role of flow pathways and teleconnections as  
779 factors that can have a deep influence in the variations in atmospheric composition at a site  
780 located in the central Mediterranean. This was possible since the time series of data acquired at  
781 the station was long enough to characterize a sort of short-term climatology of the site. The  
782 results are therefore of paramount importance to better understand processes controlling the  
783 variability of atmospheric composition in a region recognized as a hotspot of air pollution and  
784 climate change.

## 785 **Acknowledgments and Data**

786 The authors would like to gratefully thank Dr. Scott Chambers from ANSTO and an anonymous reviewer  
787 for providing constructive comments during the review process, which overall contributed to improve the  
788 quality of the manuscript. CAMM Monte Cimone by Italian Air Force and ISAC-CNR are gratefully  
789 acknowledged for their precious technical support at the Mt. Cimone station and for the help in the  
790 collection of compositional datasets, and in particular for providing data of meteorological and  
791 atmospheric composition data useful for this research. ISAC-CNR is gratefully acknowledged for  
792 providing aerosol size distribution, black carbon and ozone data, besides infrastructural access at the  
793 WMO-GAW Global Station Italian Climate Observatory "O. Vittori" at Mt. Cimone.  
794 IAFMS is gratefully acknowledged for providing meteorological and carbon dioxide data.

795 World Data Centre for Greenhouse Gases (<https://gaw.kishou.go.jp/>) and EBAS databases  
 796 (<http://ebas.nilu.no/>) are acknowledged for making available ozone, carbon dioxide, carbon monoxide,  
 797 fine and coarse particle number density and black carbon data useful for this research work.  
 798 We acknowledge NOAA (<http://www.esrl.noaa.gov/>) for providing the HYSPLIT trajectory model  
 799 (available at <http://ready.arl.noaa.gov/HYSPLIT.php>) and the NCEP/NCAR reanalysis data used in this  
 800 study. NOAA/ESRL Physical Sciences Division, Boulder Colorado is also acknowledged for providing  
 801 daily images of meteorological variables (available at <http://www.esrl.noaa.gov/psd/>) useful for this  
 802 research.  
 803 The University of Wyoming (<http://weather.uwyo.edu/upperair/sounding.html>) and NASA Goddard Earth  
 804 Sciences Data and Information Services Center (<http://mirador.gsfc.nasa.gov>) are acknowledged for  
 805 providing soundings and satellite data.  
 806 James Hurrell and the National Center for Atmospheric Research staff are acknowledged for providing  
 807 NAO indices (both station and Principal Component-based) data and metadata retrieved from  
 808 <https://climatedataguide.ucar.edu/climate-data/hurrell-north-atlantic-oscillation-nao-index-station-based>.  
 809 Tim Osborn and CRU staff are acknowledged for providing NAO indices based on the difference  
 810 between the sea level pressure over Gibraltar and the sea level pressure over Southwest Iceland retrieved  
 811 from <https://crudata.uea.ac.uk/cru/data/nao/>  
 812 Erika Brattich thanks the University Miguel Hernandez de Elche and Prof. Orza for giving her the  
 813 possibility of a three months research period to start the collaboration which posed the scientific basis of  
 814 this work.  
 815 A description of the observational data used in this work is available in Sect. 2 and they are available  
 816 upon request by contacting Prof. Laura Tositti ([laura.tositti@unibo.it](mailto:laura.tositti@unibo.it)) for radionuclides observations, and  
 817 by MOVIDA – Multistation system (<http://shiny.bo.isac.cnr.it:3838/plot-multistats-en/>), implemented  
 818 under the Project of National Interest NextData) for other surface atmospheric variables observations.

## 819 References

- 820 Aebischer, U., & Schär, C., 1998. Low-Level Potential Vorticity and Cyclogenesis to the Lee of the Alps.  
 821 Journal of the Atmospheric Sciences, 55, 186-207. doi:10.1175/1520-  
 822 14691998055<0186:LLPVAC>2.0.CO;2
- 823 Añel, J.A., Gimeno, L., de la Torre L., & Nieto, R., 2006. Changes in tropopause height for the Eurasian  
 824 region determined from CARDS radiosonde data. Naturwissenschaften, 93, 603-609.  
 825 doi:10.1007/s00114-006-0147-5
- 826 Angulo-Martínez, M., & Beguería, S., 2012. Do atmospheric teleconnection patterns influence rainfall  
 827 erosivity? A study of NAO, MO and WeMO in NE Spain, 1955-2006. Journal of Hydrology, 450-  
 828 451, 168-179. doi:10.1016/j.jhydrol.2012.04.063
- 829 Arimoto, R., Snow, J.A., Graustein, W.C., Moody, J.L., Ray, B.J., Duce, R.A., Turekian, K.K., & Maring,  
 830 H.B., 1999. Influences of atmospheric transport pathways on radionuclide activities in aerosol  
 831 particles from over the North Atlantic. Journal of Geophysical Research, 104, D17, 301-321.  
 832 doi:10.1029/1999JD900356
- 833 Balkanski, Y.J., Jacob, D.J., Gardner, G.M., Graustein, W.C., & Turekian, K.K., 1993. Transport and  
 834 residence times of tropospheric aerosols inferred from a global three-dimensional simulation of  
 835 <sup>210</sup>Pb. Journal of Geophysical Research, 98, 20573-20586. doi:10.1029/93JD02456
- 836 Barmpadimos, I., Hueglin, C., Keller, J., Henne, S., & Prévôt, A.S.H., 2011. Influence of meteorology on  
 837 PM<sub>10</sub> trends and variability in Switzerland from 1991 to 2008. Atmospheric Chemistry and Physics,  
 838 11, 1813-1835. doi:10.5194/acp-11-1813-2011

- 839 Barmpadimos, I., Keller, J., Oderbolz, D., Hueglin, C., & Prévôt A.S.H., 2012. One decade of parallel  
840 fine PM<sub>2.5</sub> and coarse PM<sub>10</sub>-PM<sub>2.5</sub> particulate matter measurements in Europe: trends and variability.  
841 Atmospheric Chemistry and Physics, 12, 3189-3203. doi:10.5194/acp-12-3189-2012
- 842 Barnston, A.G., & Livezey, R.E., 1987. Classification, seasonality and persistence of low-frequency  
843 atmospheric circulation patterns. Monthly Weather Review 115, 1083-1126.
- 844 Baskaran, M., 2011. Po-210 and Pb-210 as atmospheric tracers and global atmospheric Pb-210 fallout: a  
845 review. Journal of Environmental Radioactivity, 102, 500-513. doi:10.1175/1520-  
846 04931987115<1083:CSAPOL<2.0.CO;2
- 847 Beer, J., McCracken, K., & von Steiger, R., 2012. Cosmogenic radionuclides. Springer, Heidelberg, pp.  
848 428.
- 849 Beine, H.J., Amoroso, A., Esposito, G., Sparapani, R., Ianniello, A., Georgiadis, T., Nardino, M.,  
850 Bonasoni, P., et al. 2005. Deposition of atmospheric nitrous acid on alkaline snow surfaces.  
851 Geophysical Research Letters, 32, L10808. doi:10.1029/2005GL022589
- 852 Bonasoni, P., Evangelisti, F., Bonafé, U., Feldmann, H., Memmesheimer, M., Stohl, A., & Tositti, L.,  
853 1999. Stratosphere-troposphere exchanges: case studies recorded at Mt. Cimone during VOTALP  
854 project. Physics and Chemistry of the Earth, Part C: Solar, Terrestrial and Planetary Science, I 245,  
855 443-446. doi:10.1016/S1464-19179900069-0
- 856 Bonasoni, P., Stohl, A., Cristofanelli, P., Calzolari, F., Colombo, T., & Evangelisti, F., 2000a.  
857 Background ozone variations at Mt Cimone station. Atmospheric Environment, 34, 5183-5189.  
858 doi:10.1016/S1352-23100000268-5
- 859 Bonasoni, P., Evangelisti, F., Bonafé, U., Ravegnani, F., Calzolari, F., Stohl, A., Tositti, L., Tubertini, O.,  
860 et al. 2000b. Stratospheric ozone intrusion episodes recorded at Mt. Cimone during VOTALP  
861 project: Case studies. Atmospheric Environment, 34, 1355-1365. doi:10.1016/S1352-23109900280-0
- 862 Brankov, E., Rao, S.T., & Porter, P.S., 1998. A trajectory-clustering correlation methodology for  
863 examining the long-range transport of air pollutants. Atmospheric Environment 32 9, 1525-1534.  
864 doi:10.1016/S1352-23109700388-9
- 865 Brattich, E., Hernández-Ceballos, M.A., Cinelli, G., & Tositti L., 2015a. Analysis of <sup>210</sup>Pb peak values at  
866 Mt. Cimone 1998-2011. Atmospheric Environment, 112, 136-147.  
867 doi:10.1016/j.atmosenv.2015.04.020
- 868 Brattich, E., Riccio, A., Tositti, L., Cristofanelli, P., & Bonasoni, P., 2015b. An outstanding Saharan Dust  
869 event at Mt. Cimone 2165 m asl, Italy in March 2004. Atmospheric Environment, 113, 223-235.  
870 doi:10.1016/j.atmosenv.2015.05.017
- 871 Brattich, E., Hernández-Ceballos, M.A., Orza, J.A.G., Bolívar, J.P., & Tositti, L., 2016. The western  
872 Mediterranean basin as an aged aerosols reservoir: insights from an old-fashioned but efficient  
873 radiotracer. Atmospheric Environment, 141, 481-493. doi:10.1016/j.atmosenv.2016.07.022
- 874 Brattich, E., Orza, J.A.G., Cristofanelli, P., Bonasoni, P., & Tositti, L., 2017a. Influence of stratospheric  
875 air masses on radiotracers and ozone over the central Mediterranean. Journal of Geophysical  
876 Research: Atmospheres, 12213, 7164-7182. doi:10.1002/2017JD027036
- 877 Brattich, E., Liu, H., Tositti, L., Considine, D.B., & Crawford, J.H., 2017b. Processes controlling the  
878 seasonal variations in <sup>210</sup>Pb and <sup>7</sup>Be at the Mt. Cimone WMO-GAW global station, Italy: a model  
879 analysis. Atmospheric Chemistry and Physics, 17, 1061-1080. doi:10.5194/acp-17-1061-2017
- 880 Brunetti, M., Maugeri, M., & Nanni, T., 2002. Atmospheric circulation and precipitation in Italy for the  
881 last 50 years. International Journal of Climatology, 22, 1455-1471. doi:10.1002/joc.805

- 882 Bueh, C., & Nakamura, Y., 2007. Scandinavian pattern and its climatic impact. *Quarterly Journal*  
883 *of the Royal Meteorological Society*, 133, 2117-2131, doi:10.1002/qj.173
- 884 Cabello, M., Orza, J.A.G., & Galiano, V., 2008a. Influence of meteorological input data on backtrajectory  
885 cluster analysis-a seven-year study for southeastern Spain. *Advances in Science and Research*, 2, 65-  
886 70. doi:10.5194/asr-2-65-2008
- 887 Cabello, M., Orza, J.A.G., & Galiano, V., 2008b. Air mass origin and its influence over the aerosol size  
888 distribution: a study in SE Spain. *Advances in Science and Research*, 2, 47-52. doi:10.5194/asr-2-47-  
889 2008
- 890 Chambers, S.D., Zahorowski, W., Williams, A.G., Crawford, J., & Griffiths, A.D., 2013. Identifying  
891 tropospheric baseline air masses at Mauna Loa Observatory between 2004 and 2010 using Radon-  
892 222 and back trajectories. *Journal of Geophysical Research Atmospheres*, 118,  
893 doi:10.1029/2012JD018212
- 894 Chambers, S.D., Hong, S.-B., Williams, A.G., Crawford, J., Griffiths, A.D., & Park, S.-J., 2014.  
895 Characterising terrestrial influence on Antarctic air masses using Radon-222 measurements at King  
896 George Island. *Atmospheric Chemistry and Physics*, 14, 9903-9916, doi:10.5194/acpd-14-11541-  
897 2014
- 898 Chambers, S.D., Williams, A.G., Conen, F., Griffiths, A.D., Reimann, S., Steinbacher, M., Krummel,  
899 P.B., Steele, L.P., van der Shoot, M.V., Galbally, I.E., Molloy, S.B., & Barnes, J.E., 2016a. Towards  
900 a universal “baseline” characterization of air masses for high- and low-altitude observing stations  
901 using ‘Radon-222’. *Aerosol and Air Quality Research*, 16, 885-899, doi:10.4209/aaqr.2016.06.0391
- 902 Chambers, S.D., Kang, C.-H., Williams, A.G., Crawford, J., et al., 2016b. Improving the representation of  
903 cross-boundary transport of anthropogenic pollution in East Asia using Radon-222. *Aerosol and Air*  
904 *Quality Research* 16, 958-976, doi: 10.4209/aar.2015.08.0522
- 905 Ciattaglia, L., 1983. Interpretation of Atmospheric CO<sub>2</sub> measurements at Mt. Cimone Italy Related to  
906 Wind Data. *Journal of Geophysical Research*, 88, C2, 1331-1338. doi:10.1029/JC088iC02p01331
- 907 Ciattaglia, L., Cundari, V., & Colombo, T., 1987. Further measurements of atmospheric carbon dioxide at  
908 Mt. Cimone, Italy: 1979-1985. *Tellus B*, 39, 1-2, 13-20. doi:10.3402/tellusb.v39i1-2.15319
- 909 Cleveland, R.B., Cleveland, W.S., McRae, J.E., & Terpenning, I., 1990. STL: A seasonal-trend  
910 decomposition procedure based on Loess. *Journal of Official Statistics* 6, 3–73.
- 911 Colette, A., Granier, C., Hodnebrog, Ø., Jakobs, H., Maurizi, A., Nyiri, A., Bessagnet, B., D’Angiola, A.,  
912 et al., 2011. Air quality trends in Europe over the past decade: a first multi-model assessment.  
913 *Atmospheric Chemistry and Physics*, 11, 11657-11678. doi:10.5194/acp-11-11657-2011
- 914 Colombo, T., Santaguida, R., Capasso, A., Calzolari, F., Evangelisti, F., & Bonasoni P., 2000. Biospheric  
915 influence on carbon dioxide measurements in Italy. *Atmospheric Environment*, 34, 4963-4969.  
916 doi:10.1016/S1352-231000000366-6
- 917 Conte, M., Giuffrida, S., & Tedesco, S., 1989. The Mediterranean oscillation: impact on precipitation and  
918 hydrology in Italy. In: *Proceedings of the Conference on Climate and Water*, Vol. 1. Publications of  
919 Academy of Finland: Helsinki, pp. 121-137.
- 920 Cristofanelli, P., Bonasoni, P., Collins, W., Feichter, J., Forster, C., James, P., Kentarchos, A., Kubik,  
921 P.W., et al. 2003. Stratosphere-to-troposphere transport: A model and method evaluation. *Journal of*  
922 *Geophysical Research*, 108, D12, 8525. doi:10.1029/2002JD002600
- 923 Cristofanelli, P., Bonasoni, P., Tositti, L., Bonafé, U., Calzolari, F., Evangelisti, F., Sandrini, S., & Stohl,  
924 A., 2006. A 6-year analysis of stratospheric intrusions and their influence on ozone at Mt. Cimone

- 2165 m above sea level. *Journal of Geophysical Research*, 111, D03306.  
doi:10.1029/2005JD006553.
- 927 Cristofanelli, P., Bonasoni, P., Carboni, G., Calzolari, F., Casarola, L., Zauli Sajani, S., & Santaguida R.,  
928 2007. Anomalous high ozone concentrations recorded at a high mountain station in Italy in summer  
929 2003. *Atmospheric Environment* 41, 1383-1394. doi:10.1016/j.atmosenv.2006.10.017
- 930 Cristofanelli, P., Calzolari, F., Bonafé, U., Duchi, R., Marinoni, A., Roccatò, F., Tositti, L., & Bonasoni,  
931 P., 2009a. Stratospheric intrusion index  $SI^2$  from baseline measurement data. *Theoretical and*  
932 *Applied Climatology*, 97, 317-325. doi:10.1016/j.atmosenv.2006.10.017
- 933 Cristofanelli, P., Marinoni, A., Arduini, J., Bonafé, U., Calzolari, F., Colombo, T., Decesari, S., Duchi,  
934 R., et al., 2009b. Significant variations of trace gas composition and aerosol properties at Mt.  
935 Cimone during air mass transport from North Africa – contributions from wildfire emissions and  
936 mineral dust. *Atmospheric Chemistry and Physics*, 9, 4603-4619. doi:10.5194/acp-9-4603-2009
- 937 Cristofanelli, P., & Bonasoni, P., 2009. Background ozone in the southern Europe and Mediterranean  
938 area: Influence of the transport processes. *Environmental Pollution*, 157, 1399-1406.  
939 doi:10.1016/j.envpol.2008.09.017
- 940 Cristofanelli P., Fierli, F., Marinoni, A., Calzolari, F., Duchi, R., Burkhardt, J., Stohl, A., Maione, M., et  
941 al., 2013. Influence of biomass burning and anthropogenic emissions on ozone, carbon monoxide  
942 and black carbon at the Mt. Cimone WMO-GAW global station Italy, 2165 m asl. *Atmospheric*  
943 *Chemistry and Physics*, 13, 15-30. doi:10.5194/acp-13-15-2013
- 944 Cristofanelli P., Scheel, H.-E., Steinbacher, M., Saliba, M., Azzopardi, M., Ellul, R., Fröhlich, M., et al.,  
945 2015. Long-term surface  $O_3$  variability at Mt. Cimone WMO/GAW global station 2165 m asl, Italy.  
946 *Atmospheric Environment*, 101, 23-33. doi:10.1016/j.atmosenv.2014.11.012
- 947 Cristofanelli, P., Landi, T.C., Calzolari, F., Duchi, R., Marinoni, A., Rinaldi, M., and Bonasoni, P., 2016.  
948 Summer atmospheric composition over the Mediterranean basin: investigation on transport processes  
949 and pollutant export to the free troposphere by observations at the WMO/GAW Mt. Cimone global  
950 station Italy, 2165 m a.s.l. *Atmospheric Environment*, 141, 139-152,  
951 doi:10.1016/j.atmosenv.2016.06.048
- 952 Cristofanelli, P., Busetto, M., Calzolari, F., Ammoscato, I., Gullì, D., Dinoi, A., Calidonna, C.R., Contini,  
953 D., et al., 2017. Investigation of reactive gases and methane variability in the coastal boundary layer  
954 of the central Mediterranean basin. *Elementa Science of the Anthropocene*, 5, 12,  
955 doi:10.1525/elementa.216
- 956 Cristofanelli, P., Brattich, E., Decesari, S., Landi, T.C., Maione, M., Putero, D., Tositti, L., & Bonasoni  
957 P., 2018. High-Mountain Atmospheric Research The Italian Mt. Cimone WMO/GAW Global Station  
958 2165 m asl. *SpringerBriefs in Meteorology* ISBN 978-3-319-61126-6, doi:10.1007/978-3-319-  
959 61127-3
- 960 Cuevas, E., Gonzalez, Y., Rodríguez, S., Guerra, J.C., Gómez-Peláez, A.J., Alonso-Pérez, S., Bustos, J.,  
961 & Milford, C., 2013. Assessment of atmospheric processes driving ozone variations in the  
962 subtropical North Atlantic free troposphere. *Atmospheric Chemistry and Physics*, 13, 1973-1998.  
963 doi:10.5194/acp-13-1973-2013
- 964 Draxler, R., & Hess, G.D., 1997. Description of the HYSPLIT\_4 modeling system. NOAA Tech. Memo.  
965 ERL ARL-224 NOAA Air Resources Laboratory, Silver Spring, MD, 24 pp.
- 966 Draxler, R.R., & Hess, G.D., 1998. An overview of the HYSPLIT\_4 modeling system of trajectories,  
967 dispersion, and deposition. *Australian Meteorological Magazine*, 47, 295-308.

- 968 Draxler, R.R., Stunder, B., Rolph, G., Stein, A., & Taylor, A., 2018. HYSPLIT4 user's guide, Version 4.  
969 NOAA Air Resources Laboratory. Last revised February 2018,  
970 [https://www.arl.noaa.gov/document/reports/hysplit\\_user\\_guide.pdf](https://www.arl.noaa.gov/document/reports/hysplit_user_guide.pdf) Last accessed 11  
971 November 2019
- 972 Duchi, R., Cristofanelli, P., Landi, T.C., Arduini, J., Bonafe, U., Bourcier, L., Busetto, M., Calzolari, F.,  
973 Marinoni, A., Putero, D., and Bonasoni, P., 2016. Long-term 2002-2012 investigation of Saharan  
974 dust transport events at Mt. Cimone GAW global station, Italy 2165 m a.s.l. *Elementa Science of the*  
975 *Anthropocene*, 4, p.000085, doi:10.12952/journal.elementa.000085
- 976 Dueñas, C., Orza, J.A.G., Cabello, M., Fernández, M.C., Cañete, S., Pérez, M., & Gordo E., 2011. Air  
977 mass origin and its influence on radionuclide activities  $^7\text{Be}$  and  $^{210}\text{Pb}$  in aerosol particles at a coastal  
978 site in the western Mediterranean. *Atmospheric Research*, 101, 205-214.  
979 doi:10.1016/j.atmosres.2011.02.011
- 980 Dulac, F., Hamonou, E., Afif, C., Alkama, R., Ancona, C., Annesi-Maesano, I., Beekmann, M. &  
981 Benaissa, F., Bergametti, G., Boissard, C., Borbon, A., Bouet, C., 2016. Air quality and climate in  
982 the Mediterranean region. 10.4000/books.irdeditions.24600.
- 983 Feely, H.W., Larsen, R.J., & Sanderson, C.G., 1989. Factors that cause seasonal variations in  $^7\text{Be}$   
984 concentrations in surface air. *Journal of Environmental Radioactivity*, 9, 223-249. doi:10.1016/0265-  
985 931X-8990046-5
- 986 Fischer, H., Kormann, R., Klüpfel, T., Gurk, Ch., Königstedt, R., Parchatka, U., Mühle, J., Rhee, T.S., et  
987 al. 2003. Ozone production and trace gas correlations during the June 2000 MINATROC intensive  
988 measurement campaign at Mt Cimone. *Atmospheric Chemistry and Physics*, 3, 725-738.  
989 doi:10.5194/acp-3-725-2003
- 990 Fleming, Z.L., Monks, P.S., & Manning, A.J., 2012. Review: Untangling the influence of air-mass history  
991 in interpreting observed atmospheric composition. *Atmospheric Research*, 104-105, 1-39.  
992 doi:10.1016/j.atmosres.2011.09.009
- 993 Gaffney, J.S, Marley, N., & Cunningham, M.M., 2004. Natural radionuclides in fine aerosols in the  
994 Pittsburgh area. *Atmospheric Environment*, 38, 3191-3200. doi:10.1016/j.atmosenv.2004.03.015
- 995 Gordo, E., Liger, E., Dueñas, C., Fernandez, M., Cañete, S., & Pérez, M., 2015. Study of  $^7\text{Be}$  and  $^{210}\text{Pb}$  as  
996 radiotracers of African intrusions in Malaga Spain. *Journal of Environmental Radioactivity*, 148,  
997 141-153. doi:10.1016/j.envrad.2015.06.028
- 998 Griffiths, A.D., Conen, F., Weingartner, E., Zimmermann, L., Chambers, S.D., Williams, A.G., &  
999 Steinbacher, M., 2014. Surface-to-mountaintop transport characterised by radon observations at the  
1000 Jungfraujoeh. *Atmospheric Chemistry and Physics*, 14, 12763-12779, doi:10.5194/acp-14-12763-  
1001 2014
- 1002 Grossi, C., Ballester, J., Serrano, I., Galmarini, S., Camacho, A., Curcoll, R., Morguá, J.A., Rodó, X., et  
1003 al. 2016. Influence of long-range atmospheric transport pathways and climate teleconnection patterns  
1004 on the variability of surface  $^{210}\text{Pb}$  and  $^7\text{Be}$  in southwestern Europe. *Journal of Environmental*  
1005 *Radioactivity*, 165, 103-114, doi: 10.1016/j.jenvrad.2016.09.011
- 1006 Hernández, F., Rodríguez, S., Karlsson, L., Alonso-Pérez, S., López-Pérez, M., Hernandez-Armas, J., &  
1007 Cuevas, E., 2008. Origin of observed high  $^7\text{Be}$  and mineral dust concentrations in ambient air on the  
1008 Island of Tenerife. *Atmospheric Environment* 42, 4247-4256. doi:10.1016/j.atmosenv.2008.01.017
- 1009 Hernandez-Ceballos, M.A., Brattich, E., and Cinelli, G., 2016. Heat-wave events in Spain: air mass  
1010 analysis and impacts on  $^7\text{Be}$  concentrations. *Advances in Meteorology*, 8026018,  
1011 doi:10.115/2016/8026018

- 1012 Hirsch, R.M., Slack, J.R., & Smith, R.A., 1982. Techniques of trend analysis for monthly water quality  
1013 data. *Water Resources Research*, 181, 107–121. doi:10.1029/WR018i001p00107
- 1014 Hurrell, J.W., 1995. Decadal trends in the North Atlantic oscillation: regional temperatures and  
1015 precipitation. *Science*, 269, 676-679. doi:10.1126/science.269.5224.676
- 1016 Hurrell, J.W., 1996. Influence of variations in extratropical wintertime teleconnections on Northern  
1017 Hemisphere temperatures. *Geophysical Research Letters*, 23, 665-668. doi:10.1029/96GL00459
- 1018 Hurrell, J.W., Deser, C., 2009. North Atlantic climate variability: the role of the North Atlantic Oscillation.  
1019 *Journal of Marine Systems*, 78, 28-41.
- 1020 Hurrell, J.W., Kushnir, Y., Ottersen, G., & Visbeck, M., 2003. An overview of the North Atlantic Oscillation.  
1021 In: *The North Atlantic Oscillation: Climatic Significance and Environmental Impact*, AGU monograph  
1022 13, 1-35.
- 1023 Ioannidou, A., Vasileiadis, A., & Melas, D., 2014. Time lag between the tropopause height and  $^7\text{Be}$   
1024 activity concentrations in surface air. *Journal of Environmental Radioactivity* 129, 80-85.  
1025 doi:10.1016/j.jenvrad.2013.12.013
- 1026 Izquierdo, R., Alarcón, M., & Àvila, A., 2013. WeMO effects on the amount and the chemistry of winter  
1027 precipitation in the north-eastern Iberian Peninsula. *Tethys Journal of Weather and Climate of the*  
1028 *Western Mediterranean*, 10, 45-51. doi:10.3369/tethys.2013.10.05
- 1029 James, P., Stohl, A., Forster, C., Eckhardt, S., Seibert, P., & Frank, A., 2003. A 15-year climatology of  
1030 stratosphere-troposphere exchange with a Lagrangian particle dispersion model 2. Mean climate and  
1031 seasonal variability. *Journal of Geophysical Research*, 108D12, 8522. doi:10.1029/2002JD002639
- 1032 Jones, P.D., Jonsson, T., & Wheeler, D., 1997. Extension to the North Atlantic Oscillation using early  
1033 instrumental pressure observations from Gibraltar and South-West Iceland. *International Journal of*  
1034 *Climatology*, 17, 1433-1450. doi:10.1002/SICI1097-00881997111517:13<1433::AID-  
1035 JOC203>3.0.CO;2-P
- 1036 Jorba, O., Pérez, C., Rocadenbosch, F., & Baldasano, J.M., 2004. Cluster analysis of 4-day back-  
1037 trajectories arriving in the Barcelona Area, Spain, from 1997 to 2002. *Journal of Applied*  
1038 *Meteorology and Climatology*, 43, 887-901. doi:10.1175/1520-  
1039 04502004043<0887:CAODBT>2.0.CO;2
- 1040 Kalnay E., Kanamitsu, M., Kistler, R., Collins, W., Deaven, D., Gandin, L., Iredell, M., Saha, S., et al.,  
1041 1996. The NCEP/NCAR reanalysis 40-year project. *Bulletin of the American Meteorological*  
1042 *Society*, 77, 437-471. doi:10.1175/1520-04771996077<0437:TNYRP>2.0.CO;2
- 1043 Koch, D.M., Jacob, J., & Graustein, W.C., 1996. Vertical transport of tropospheric aerosols as indicated  
1044  $^7\text{Be}$  and  $^{210}\text{Pb}$  in a chemical tracer model. *Journal of Geophysical Research*, 101: 18651-18666.  
1045 doi:10.1029/96JD01176
- 1046 Kulan, A., Aldahan, A., Possnert, G., Vintersved, I., 2006. Distribution of  $^7\text{Be}$  in surface air of Europe.  
1047 *Atmospheric Environment*, 40, 3855-3868. doi:10.1016/j.atmosenv.2006.02.030
- 1048 Lee, H.N., Tositti, L., Zheng, X., & Bonasoni, P., 2007. Analyses and comparisons of variations of  $^7\text{Be}$ ,  
1049  $^{210}\text{Pb}$  and  $^7\text{Be}/^{210}\text{Pb}$  with ozone observations at two Global Atmosphere Watch stations from high  
1050 mountains. *Journal of Geophysical Research*, 112, D05303. doi:10.1029/2006JD007421
- 1051 Li, Q., Jacob, D.J., Fairlie, T.D., Liu, H., Martin, R.V., & Yantosca, R.M., 2002. Stratospheric versus  
1052 pollution influences on ozone at Bermuda: Reconciling past analyses. *Journal of Geophysical*  
1053 *Research*, 107, D22, 4611. doi:10.1029/2002JD002138

- 1054 Lim, Y.-K., 2015. The East Atlantic/West Russia EA/WR teleconnection in the North Atlantic: climate  
1055 impact and relation to Rossby wave propagation. *Climate Dynamics*, 44, 11-12, 3211-3222,  
1056 doi:10.1007/s00382-014-2381-4
- 1057 Lozano, R.L., Hernández-Ceballos, M.A., San Miguel, E.G., Adame, J.A., & Bolívar, J.P., 2012.  
1058 Meteorological factors influencing the <sup>7</sup>Be and <sup>210</sup>Pb concentrations in surface air from the  
1059 southwestern Iberian Peninsula. *Atmospheric Environment*, 43, 168-178.  
1060 doi:10.1016/j.atmosenv.2012.09.052
- 1061 Machta, L., 1972. Mauna Loa and global trends in air quality. *Bulletin of the American Meteorological*  
1062 *Society*, 53, 402-420. doi:10.1175/1520-04771972053<0402:MLAGTI>2.0.CO;2
- 1063 Marinoni, A., Cristofanelli, P., Calzolari, F., Roccató, F., Bonafé, U., & Bonasoni, P., 2008. Continuous  
1064 measurements of aerosol physical parameters at the Mt Cimone GAW Station 2165 m asl, Italy.  
1065 *Science of the Total Environment*, 391, 241-251. doi:10.1016/j.scitotenv.2007.10.004
- 1066 Martin-Vide, J., & Lopez-Bustins, J.-A., 2006. The Western Mediterranean Oscillation and rainfall in the  
1067 Iberian Peninsula. *International Journal of Climatology*, 26, 1455-1475. doi:10.1002/joc.1388
- 1068 Menut, L., Masson, O., & Bessagnet, R., 2009. Contribution of Saharan dust on radionuclide activity  
1069 levels on Europe? The 21-22 February 2004 case study. *Journal of Geophysical Research*, 114,  
1070 D16202. doi:10.1029/2009JD011767
- 1071 Moulin, D., Lambert, C. E., Dulac, F., & Dayan, U., 1997. Control of atmospheric export of dust from  
1072 North Africa by the North Atlantic Oscillation. *Nature*, 387, 691-694. doi:10.1038/42679
- 1073 Myhre G., Shindell, D., Bréon, F.-M., Collins, W., Fuglestedt, J., Huang, J., Koch, D., Lamarque, J.-F.,  
1074 et al., 2013. Anthropogenic and Natural Radiative Forcing. In: *Climate Change 2013: The Physical*  
1075 *Science Basis. Contribution of Working Group I to the Fifth Assessment Report of the*  
1076 *Intergovernmental Panel on Climate Change.* Stocker, T.F., Qin, D., Plattner, G.-K., Tignor, M.,  
1077 Allen, S.K., Boschung, J., Nauels, A., Xia, Y., et al. Eds. Cambridge University Press, Cambridge,  
1078 United Kingdom and New York, NY, USA.
- 1079 Ochoa-Hueso, R., Munzi, S., Alonso, R., et al., 2017. Ecological impacts of atmospheric pollution and  
1080 interactions with climate change in terrestrial ecosystems of the Mediterranean basin: current  
1081 research and future directions. *Environmental Pollution*, 227, 194-206,  
1082 doi:10.1016/j.envpol.2017.04.062
- 1083 Orza, J.A.G., Cabello, M., Galiano, V., Vermeulen, A.T., & Stein, A., 2013. The association between  
1084 NAO and the interannual variability of the tropospheric transport pathways in western Europe. In:  
1085 *Lagrangian Modeling of the Atmosphere.* Lin, J., Brunner, D., Gerbig, C., Stohl, A., Luhar, A.,  
1086 Webley, P. Eds. AGU Geophysical Monograph Vol. 200, 127-141.
- 1087 Pace, G., Meloni, D., di Sarra, A., 2005. Forest fire aerosol over the Mediterranean basin during summer  
1088 2003. *Journal of Geophysical Research* 110, D21202. doi:10.1029/2005JD005986
- 1089 Palutikof, J.P., 2003. Analysis of Mediterranean climate data: measured and modelled. In: *Mediterranean*  
1090 *Climate-Variability and Trends.* Bolle H.J. Ed.. Springer Verlag: Berlin; 133-153.
- 1091 Papayannis, A., Amiridis, V., Mona, L., Tsaknakis, G., Balis, D., Bösenberg, J., Chaikovski, A., de  
1092 Tomasi, F., et al., 2008. Systematic lidar observations of Saharan dust over Europe in the frame of  
1093 EARLINET 2000-2002. *Journal of Geophysical Research*, 113, D10204. doi:  
1094 10.1029/2007JD009028.
- 1095 Pausata, F.S.R., Pozzoli, L., Vignati, E., & Dentener, F.J., 2012. North Atlantic Oscillation and  
1096 tropospheric ozone variability in Europe: model analysis and measurements intercomparison.  
1097 *Atmospheric Chemistry and Physics*, 12, 6357-6376. doi:10.5194/acp-12-6357-2012

- 1098 Pérez, N., Pey, J., Castillo, S., Viana, M., Alastuey, A., & Querol, X., 2008. Interpretation of the  
1099 variability of levels of regional background aerosols in the Western Mediterranean. *Science of the*  
1100 *Total Environment*, 407, 527-540. doi:10.1016/j.scitotenv.2008.09.006
- 1101 Perrone, M.R., Becagli, S., Orza, J.A.G., Vecchi, R., Dinoi, A., Udisti, R., & Cabello, M., 2013. The impact of  
1102 long-range-transport on PM1 and PM2.5 at a Central Mediterranean site. *Atmospheric Environment*, 71,  
1103 176-186. doi:10.1016/j.atmosenv.2013.02.006
- 1104 Randerson, J.T., Thompson, M.V., Conway, T.J., Fung, I.Y., & Field, C.B., 1997. The contribution of  
1105 terrestrial sources and sinks to trends in the seasonal cycle of atmospheric carbon dioxide. *Global*  
1106 *Biogeochemical Cycles*, 114, 535-560. doi:10.1029/97GB02268
- 1107 Santer, B.D., Painter, J.F., Bonfils, C., Mears, C.A., Solomon, S., Wigley, T.M.L., Glecker, P.J., Schmidt,  
1108 G.A., et al. 2013. Human and natural influences on the changing thermal structure of the atmosphere.  
1109 *Proceedings of the National Academy of Sciences of the United States of America*, 110, 43, 17235-  
1110 17240. doi:10.1073/pnas.1305332110
- 1111 Sarvan, D., Stratimirović, Đ., Blesić, S., Djurdjevic, V., Miljković, V., & Ajtić, J., 2017. Dynamics of  
1112 beryllium-7 specific activity in relation to meteorological variables, tropopause height,  
1113 teleconnection indices and sunspot number. *Physica A*, 469, 813-823,  
1114 doi:10.1016/j.physa.2016.11.040
- 1115 Seierstad, I.A., Stephenson, D.B., & Kvamsto, G., 2007. How useful are teleconnection patterns for  
1116 explaining variability in extratropical storminess? *Tellus Ser. A*, 59, 170-181.
- 1117 Stohl, A., Spoichtinger-Rakowsky, N., Bonasoni, P., Feldmann, H., Memmesheimer, M., Scheel, H.E.,  
1118 Trickl, T., Hübener, S., et al. 2000. The influence of stratospheric intrusions on alpine ozone  
1119 concentrations. *Atmospheric Environment*, 34, 1323-1354. doi:10.1016/S1352-23109900320-9
- 1120 Stohl, A., Haimberger, L., Scheele, M.P., & Wernli, H., 2001. An intercomparison of results from three  
1121 trajectory models. *Meteorological Applications*, 8, 2, 127-135. doi:10.1017/S1350482701002018
- 1122 Stohl A., Bonasoni, P., Cristofanelli, P., Collins, W., Feichter, W., Frank, A., Forster, C., Gerasopoulos,  
1123 E., et al., 2003. Stratosphere-troposphere exchange: a review, and what we have learned from  
1124 STACCATO. *Journal of Geophysical Research*, 108, D12, 8516. doi:10.1029/2002JD002490
- 1125 Thoning, K.W., Tans, P.P., & Komhyr, W.D., 1989. Atmospheric carbon dioxide at Mauna Loa  
1126 Observatory: 2. Analysis of the NOAA GMCC data, 1974-1985. *Journal of Geophysical Research:*  
1127 *Atmospheres*, 94D6. DOI:10.1029/JD094iD06p08549
- 1128 Tositti, L., Brattich, E., Cinelli, G., Previti, A., Mostacci, D., 2012. Comparison of radioactivity data  
1129 measured in PM10 aerosol samples at two elevated stations in northern Italy during the Fukushima  
1130 event. *Journal of Environmental Radioactivity*, 114, 105-112. doi:10.1016/j.jenvrad.2012.01.016
- 1131 Tositti, L., Riccio, A., Sandrini, S., Brattich, E., Baldacci, D., Parmeggiani, S., Cristofanelli, P., &  
1132 Bonasoni, P., 2013. Short-term climatology of PM10 at a high altitude background station in  
1133 southern Europe. *Atmospheric Environment*, 65, 145-152. doi:10.1016/j.atmosenv.2012.10.051
- 1134 Tositti, L., Brattich, E., Cinelli, G., Baldacci, D., 2014. 12 years of <sup>7</sup>Be and <sup>210</sup>Pb data in Mt. Cimone, and  
1135 their correlation with meteorological parameters. *Atmospheric Environment*, 87C, 108-122.  
1136 doi:10.1016/j.atmosenv.2014.01.014
- 1137 Trigo, R., Xoplaki, E., Lüterbacher, J., Krichak, S.O., Alpert, P., Jacobeit, J., Sáenz, J., Fernández, J.,  
1138 González-Rouco, F., et al., 2006. Relations between variability in the Mediterranean region and mid-  
1139 latitude variability. In: *Mediterranean Climate Variability*. Chapter 3, pp. 179-226. Lionello, P.,  
1140 Malanotte-Rizzoli, P., Boscolo, R. Eds. Elsevier, ISBN 978-0-444-52170-5. doi:10.1016/S1571-  
1141 91970680006-6
- 1142 Turekian, K.K., Nozki, Y., & Benninger, L.K., 1977. Geochemistry of atmospheric radon and radon  
1143 products. *Annual Review of Earth and Planetary Science*, 5, 227-255.

- 1144 Usoskin, I., & Kovaltsov, G., 2008. Production of cosmogenic  $^7\text{Be}$  isotope in the atmosphere: full 3D  
1145 modelling. *Journal of Geophysical Research* 113, D12107. doi:10.1029/2007JD009725
- 1146 Yue, S., Pilon, P., Phinney, P., & Cavadias, G., 2002. The influence of autocorrelation on the ability to  
1147 detect trend in hydrological series. *Hydrological Processes* 169, 1807-1829. doi:10.1002/hyp.1095
- 1148 Wallace, J.M., & Gutzler, D.S., 1981. Teleconnections in the geopotential height field during the  
1149 Northern Hemisphere winter. *Monthly Weather Review*, 109, 784-812.
- 1150 Wilks, D., 2011. *Statistical methods in the Atmospheric Sciences*, Volume 100. International Geophysics  
1151 Series. Third Edition Academic Press. ISBN-13: 978-0123850225
- 1152 WMO World Meteorological Organization, 2007. *Scientific Assessment on Ozone Depletion. 2006,*  
1153 *Global Ozone Research Monitoring Project-Report, No.50, Geneva Switzerland.*
- 1154 WMO World Meteorological Organization-GAW Global Atmosphere Watch, 2017. *WMO Greenhouse*  
1155 *Gas Bulletin. The state of Greenhouse Gases in the Atmosphere Based on Global Observations*  
1156 *through 2016. ISSN 2078-0796*
- 1157

1158 **Tables**

1159

1160 **Table 1.** Analysed teleconnection with associated location of centers of action including the sign  
 1161 of geopotential height (or pressure) anomalies for their positive phases.  
 1162

TELECONNECTION	ABBREVIATION	CENTERS OF ACTION
<b>NORTH ATLANTIC OSCILLATION</b>	NAO	Greenland (-), Azores (+)
<b>EAST ATLANTIC</b>	EA	North Atlantic (-), Subtropical North Atlantic and Mediterranean (+)
<b>EAST ATLANTIC/WESTERN RUSSIA</b>	EA/WR	NW Europe (+), Western Russia (-), NE China (+)
<b>SCANDINAVIA</b>	SCA	SW Europe (-), Scandinavia (+), Kazakhstan/Mongolia (-)
<b>MEDITERRANEAN OSCILLATION</b>	MO	Algiers (+), Cairo (-), Gibraltar (+), Israel (-)
<b>WESTERN MEDITERRANEAN OSCILLATION</b>	WeMO	Po Valley (-), Gulf of Cadiz (+)

1163

1164

1165

1166

1167

1168

1169

1170

1171

1172

1173

1174

1175

1176

1177

1178

1179

1180

1181

1182

1183

1184

1185

1186

1187 **Table 2.** Results of the seasonal Kendall test for the monthly time series and the trend-free pre-  
 1188 whitening Yue-Pilon (Y-P) procedure on the de-seasonalized monthly series for the detection of  
 1189 monotonic trends applied on the 1999-2006 time series. For each case, the p (significance) value  
 1190 and the mean change per year from the Theil-Sen slope are presented. In bold when significant at  
 1191 the 0.05 level, in italic when the trend is only weakly significant, i.e., at the 0.1 level.  
 1192

MONTHLY FREQUENCIES				
INDEX	Seasonal Kendall		Deseasonalized Y-P	
	p value	mean change per year	p value	mean change per year
Hurrell_Stat_NAOi	0.6935	-0.07	0.3220	-0.08
Hurrell_PC_NAOi	0.2840	-0.05	0.3645	-0.05
CPC_Stat_NAOi	0.2110	-0.07	0.1307	-0.06
CRU_Stat_NAOi	0.4320	-0.07	0.4215	+0.04
WeMOi	<b>0.0000</b>	-0.15	<b>0.0000</b>	-0.17
MOi1	0.2530	+0.01	0.2497	+0.01
MOi2	0.6171	-0.01	0.1668	-0.01
EA	0.7206	+0.02	0.9028	+0.01
EA/WR	1.0000	-0.03	0.3612	-0.03
SCA	1.0000	+0.01	0.8875	+0.01
FLOW TYPE	Seasonal Kendall		Deseasonalized Y-P	
	p value	mean change per year	p value	mean change per year
A	<b>0.0383</b>	0.000	<b>0.0462</b>	+0.007
E	0.0760	+0.003	0.1358	+0.007
Me-AF	0.8284	+0.003	0.3924	+0.001
W	<b>0.0376</b>	-0.010	<b>0.0274</b>	-0.011
Atl	0.1061	-0.006	<b>0.0349</b>	-0.007
N-Am	0.0689	0.000	0.2872	-0.003
N-Atl	0.1605	-0.004	0.3462	-0.004
NW-Eu	0.7203	+0.003	0.9232	0.000
Monthly medians				
VARIABLE	Seasonal Kendall		Deseasonalized Y-P	
	p value	mean change per year	p value	mean change per year
p (mbar)	0.1237	+0.317	0.2317	+0.133
T (°C)	0.1855	+0.300	0.1024	+0.168
RH (%)	0.1234	+0.263	0.4996	-0.336
TH (m)	0.7690	+19.296	0.9919	-10.414
ws (m s <sup>-1</sup> )	0.1336	+0.054	0.2292	+0.117
Prec (mm)	0.6408	+0.000	0.7777	+0.000
MixHeight (mm)	0.9083	+4.822	0.6875	-3.568
O <sub>3</sub> (ppbv)	0.1320	+0.279	0.1806	+0.292

<b>CO<sub>2</sub> (ppm)</b>	<b>0.0000</b>	+1.804	<b>0.0000</b>	+1.900
<b><sup>7</sup>Be (mBq m<sup>-3</sup>)</b>	0.2840	-0.079	0.1984	-0.085
<b><sup>210</sup>Pb (mBq m<sup>-3</sup>)</b>	<b>0.0450</b>	-0.008	<b>0.0135</b>	-0.011
<b>PM<sub>10</sub> (μg m<sup>-3</sup>)</b>	<b>0.0053</b>	-0.154	<b>0.0083</b>	-0.296
<b><sup>7</sup>Be/PM<sub>10</sub> (mBq μg<sup>-1</sup>)</b>	0.1851	+0.007	0.1616	+0.012
<b><sup>210</sup>Pb /PM<sub>10</sub> (mBq μg<sup>-1</sup>)</b>	0.7921	0.000	0.9839	+0.000
<b><sup>7</sup>Be/<sup>210</sup>Pb</b>	0.6678	0.000	0.3612	+0.083

1193

1194

1195

1196

1197

1198

1199

1200

1201

1202

1203

1204

1205

1206

1207

1208

1209

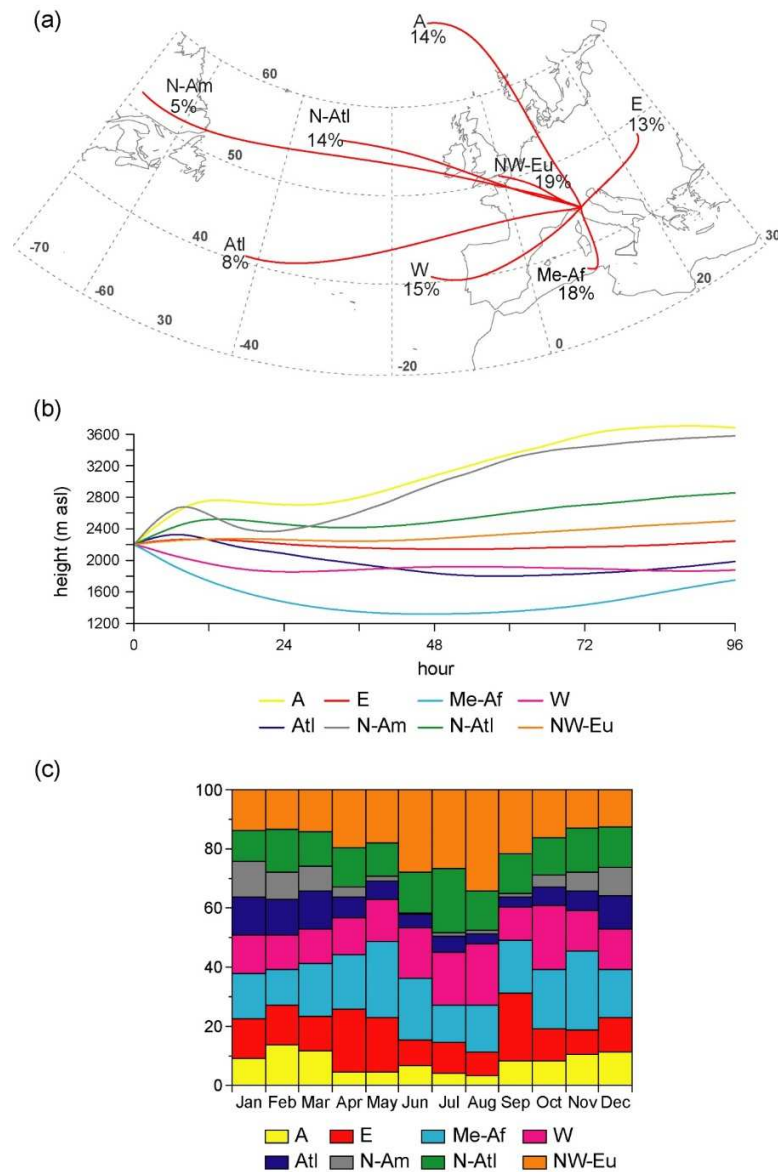
1210

1211

1212

1213

1214

1215 **Figures**

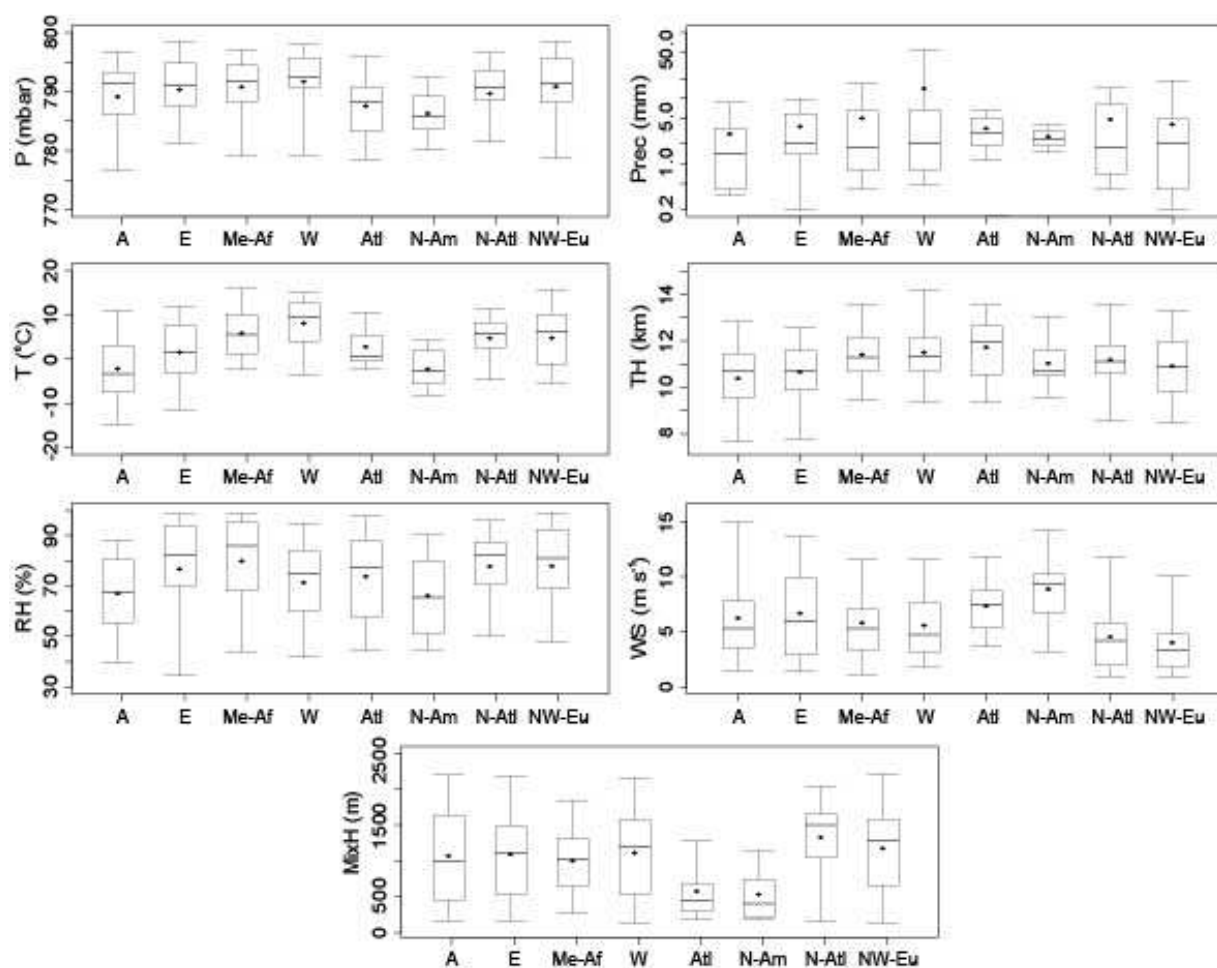
1216

1217 **Figure 1.** (a) Centroids of the trajectory clusters identified for 96-h back-trajectories arriving at  
 1218 2200 m asl for the 12-year study period. The flow pathways are identified as follows: Arctic (A),  
 1219 Eastern (E), Mediterranean-Africa (Me-AF), Atlantic (Atl), Northern Atlantic (N-Atl), North  
 1220 America (N Am), North Western-Europe (NW-Eu). The percentage is for the frequency of  
 1221 occurrence of each flow pattern in the whole 1998-2011 period. (b) Heights above mean sea  
 1222 level of the representative back-trajectories vs. end-point time. (c) Monthly variation in  
 1223 percentage frequency of the identified advection pathways.

1224

1225

1226



1227  
1228

1229 **Figure 2.** Box plots of meteorological variables measured at Mt. Cimone (P = pressure, T =  
1230 temperature, RH = relative humidity, Prec = precipitation, TH = tropopause height, WS = wind  
1231 speed, MixH = mixing height) versus air flows arriving at the receptor site. The horizontal bold  
1232 line in each box represents the 50<sup>th</sup> percentile (median), the circle represents the mean value,  
1233 lower and upper boundaries locate the 5<sup>th</sup> and 95<sup>th</sup> percentile of the values and whiskers locate  
1234 the minimum and maximum values.  
1235

1236

1237

1238

1239

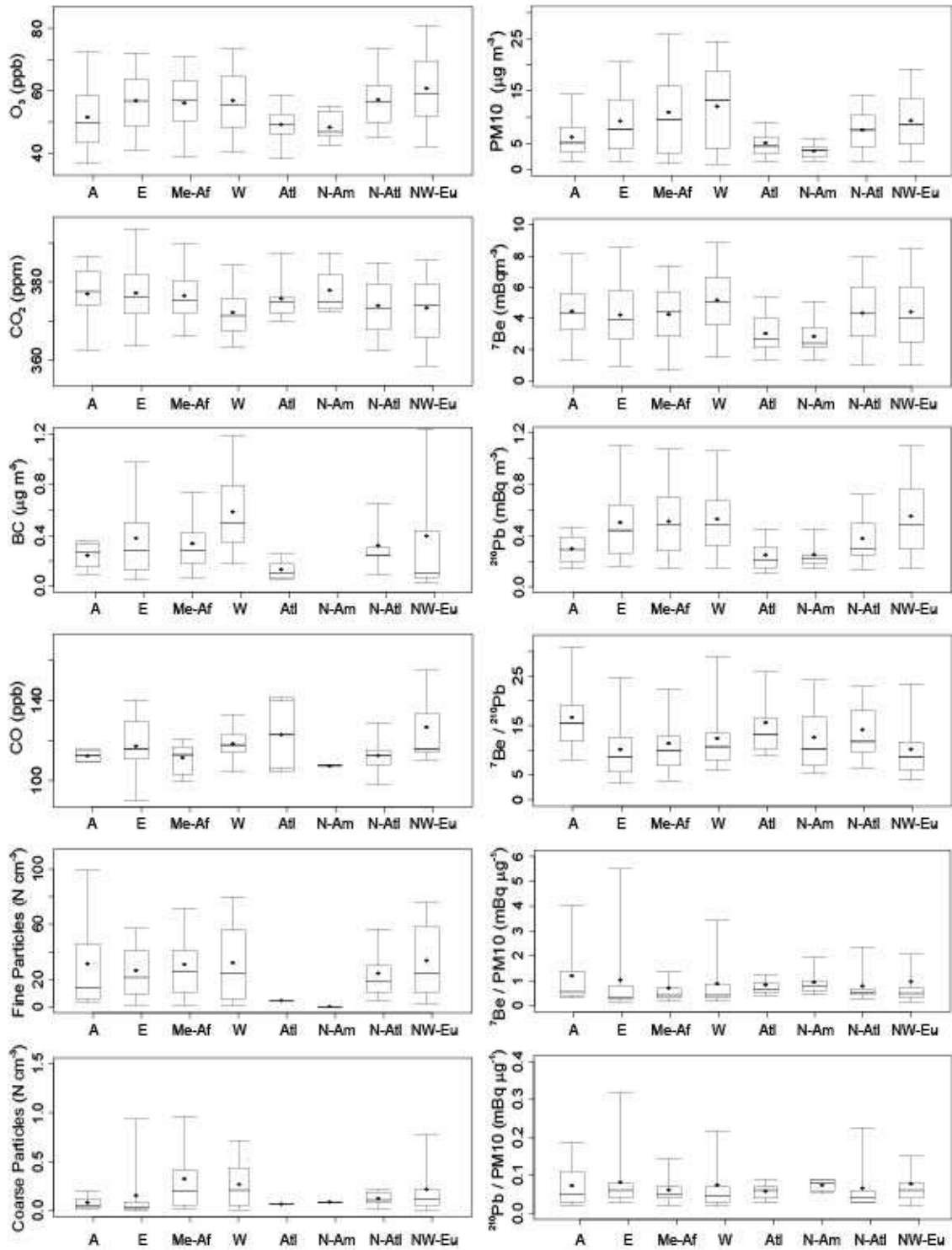
1240

1241

1242

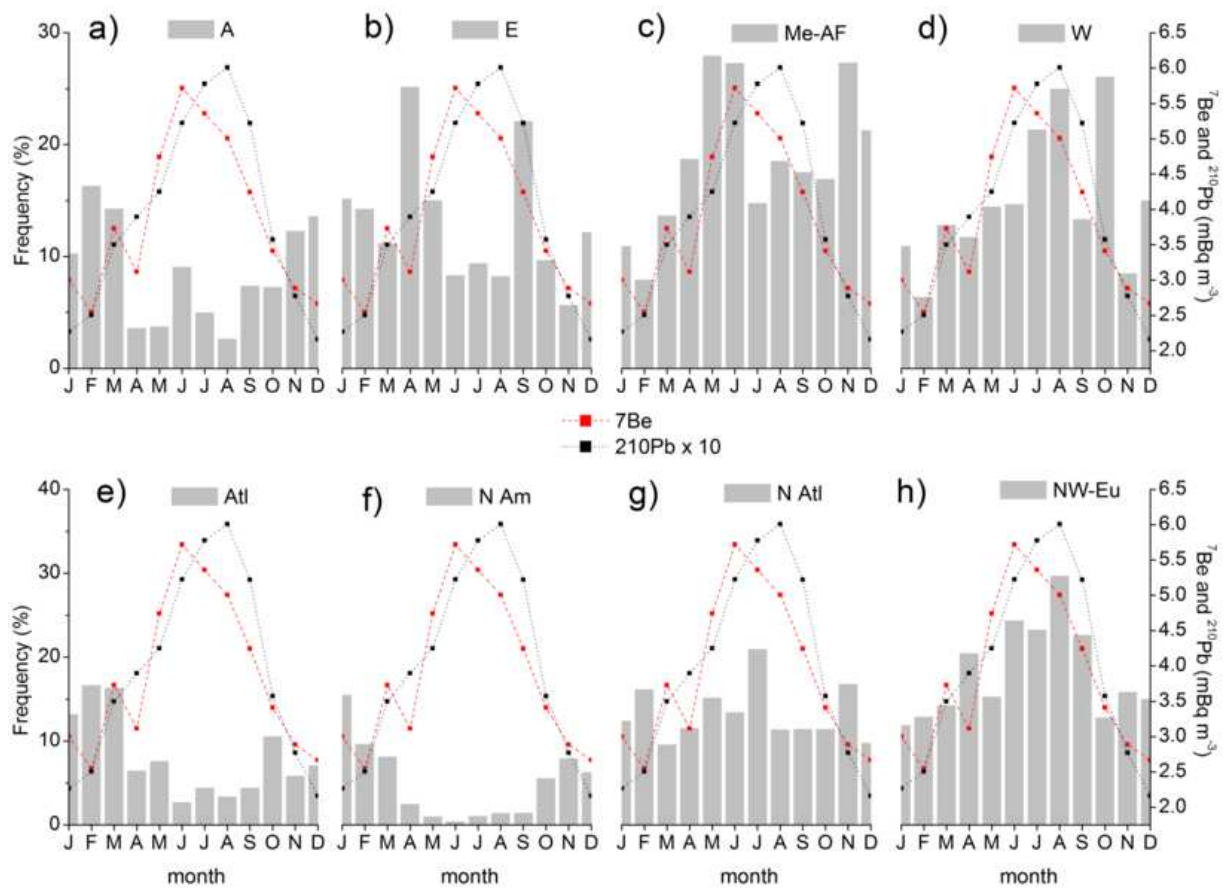
1243

1244



1245

1246 **Figure 3.** Same as Figure 2, but for atmospheric gases ( $O_3$ ,  $CO_2$ ,  $CO$ ), black carbon (BC), fine  
 1247 and coarse particles number density,  $PM_{10}$ , atmospheric radiotracers  ${}^7Be$  and  ${}^{210}Pb$ , ratio  
 1248  ${}^7Be/{}^{210}Pb$ , ratio  ${}^7Be/PM_{10}$ , ratio  ${}^{210}Pb/PM_{10}$ , versus air flows arriving at the receptor site.  
 1249



1250

1251 **Figure 4.** Monthly median activities of  $^7\text{Be}$  (right scale, red line) and  $^{210}\text{Pb}$  (right scale, black  
 1252 line) and their relationship with the monthly frequency of air flows (left scale, grey bar) at Mt.  
 1253 Cimone from: a) Arctic; b) East; c) Mediterranean-Africa; d) West; e) Atlantic; f) North  
 1254 America; g) North Atlantic; h) North Western-Europe

1255

1256

1257

1258

1259

1260

1261

1262

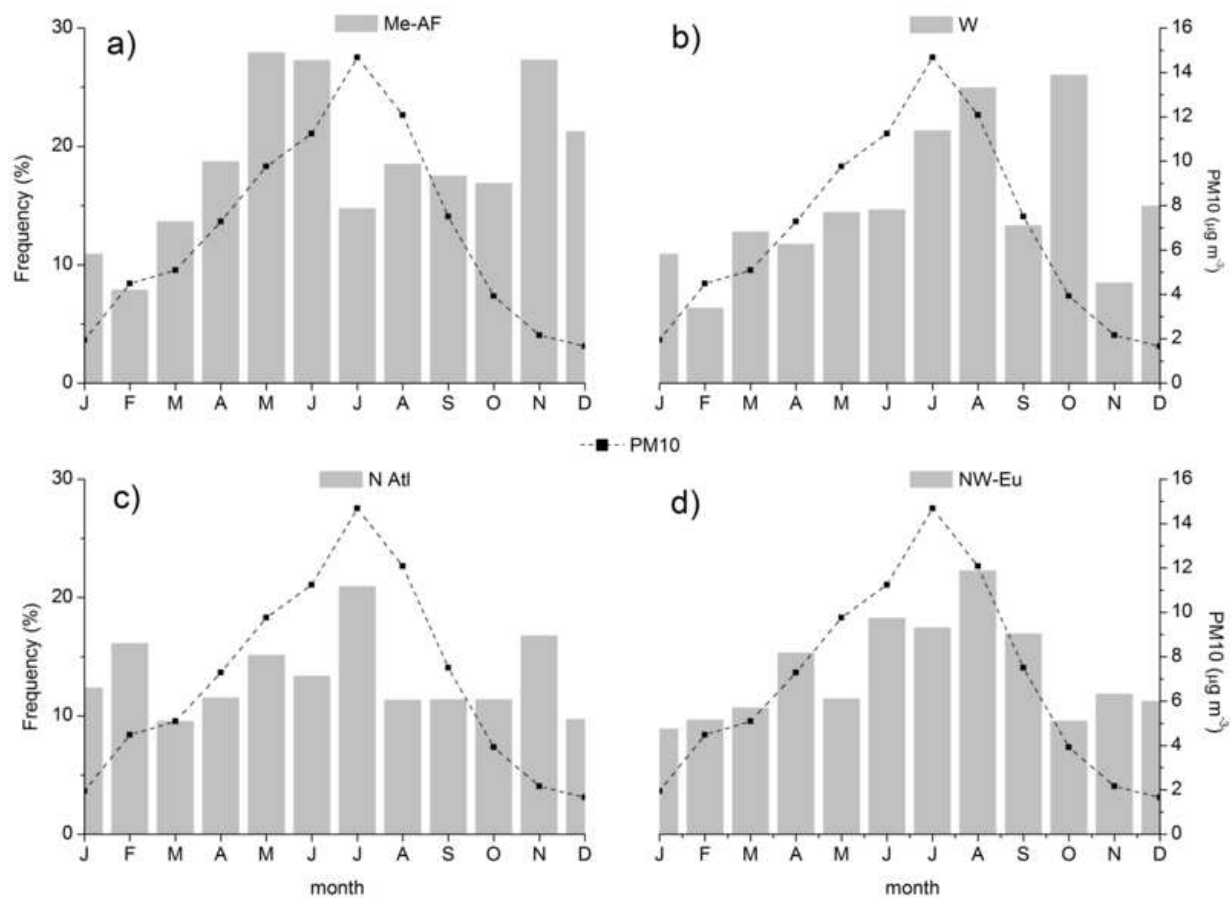
1263

1264

1265

1266

1267



1268  
1269

1270 **Figure 5.** Monthly median concentrations of PM<sub>10</sub> (right scale, black dashed line) and  
1271 relationship with the monthly frequency of air flows (left scale, grey column) at Mt. Cimone  
1272 from: a) Mediterranean-Africa; b) West; c) North Atlantic; d) North Western-Europe.  
1273

1274

1275

1276

1277

1278

1279

1280

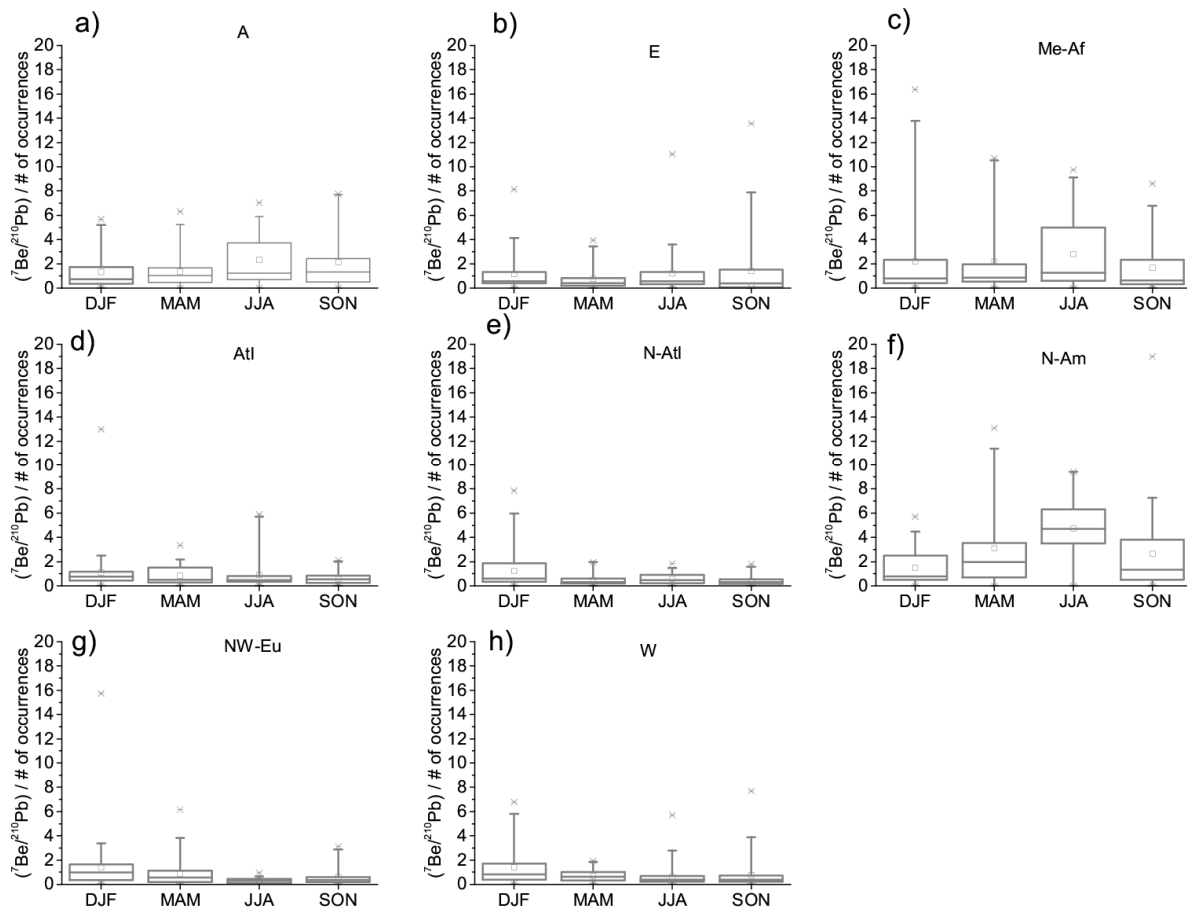
1281

1282

1283

1284

1285



1286

1287 **Figure 6.** Seasonal (DJF = December-January-February; MAM = March-April-May; JJA =  
 1288 June-July-August; SON = September-October-November; i.e., winter, spring, summer and  
 1289 autumn seasons in the Northern Hemisphere) boxplots showing the contribution to  ${}^7\text{Be}/{}^{210}\text{Pb}$  per  
 1290 number of events of each flow type: a) Arctic; b) Eastern; c) Mediterranean-Africa; d)  
 1291 Atlantic; e) North-Atlantic; f) North-America; g) North Western-Europe; h) Western. The horizontal bold  
 1292 line in each box represents the 50<sup>th</sup> percentile (median), the square represents the mean value,  
 1293 lower and upper boundaries locate the 25<sup>th</sup> and 75<sup>th</sup> percentile of the values and whiskers locate  
 1294 the 5<sup>th</sup> and 95<sup>th</sup> percentile values. Crosses and horizontal lines outside the boxes further indicate  
 1295 1<sup>st</sup> and 99<sup>th</sup> percentile and minimum and maximum values, respectively.

1296

1297

1298

1299

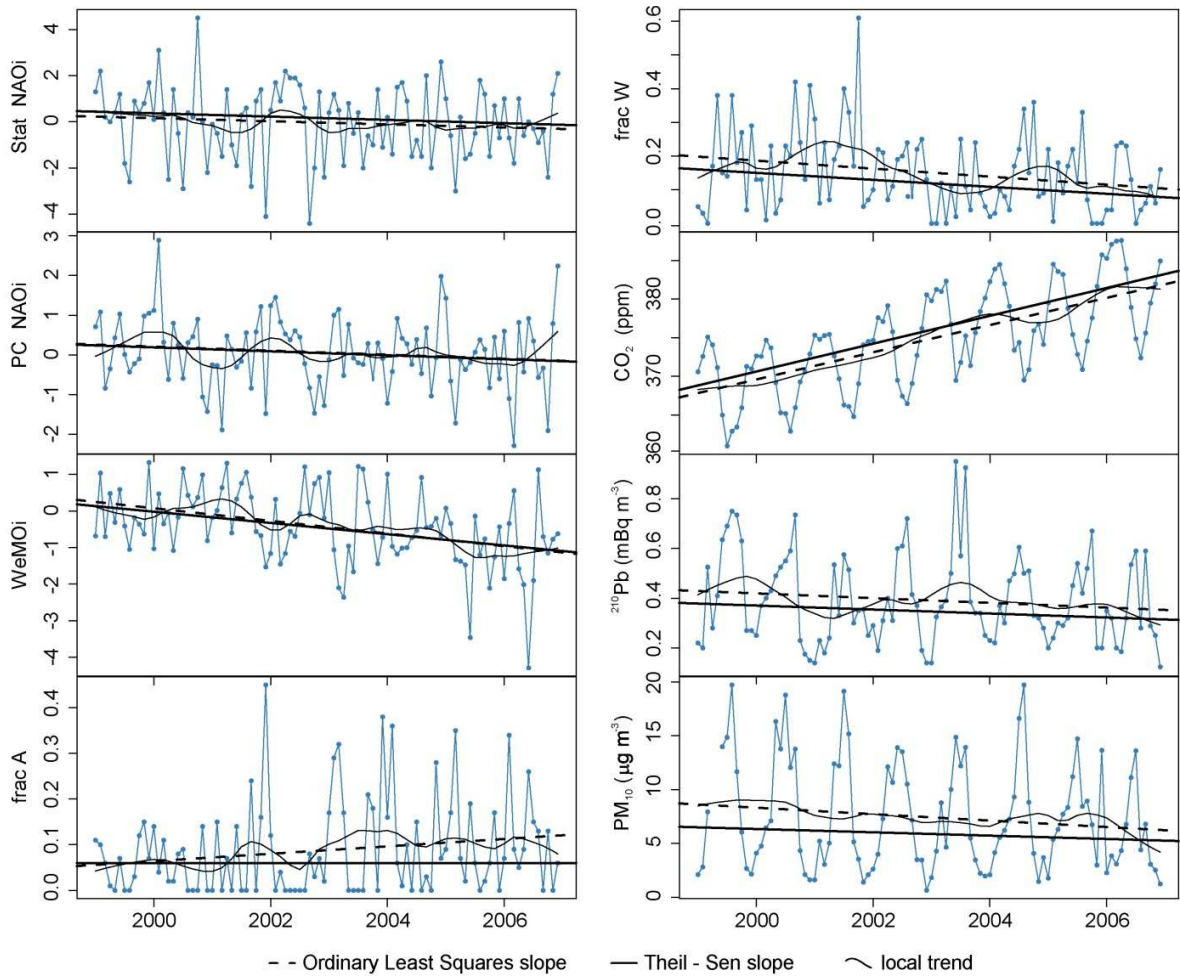
1300

1301

1302

1303

1304



1305

1306 **Figure 7.** Evolution of the monthly frequency of occurrence of the Hurrell station- and principal  
 1307 components-based NAO, WeMO indices, of the Arctic and Western flow types, and of the  
 1308 monthly medians of variables which show significant trends, over the period 1999-2006 ( $\text{CO}_2$ ,  
 1309  $^{210}\text{Pb}$  and  $\text{PM}_{10}$ ). Dashed lines are the linear regressions, solid lines are the Theil-Sen slope  
 1310 estimates, and black solid curved lines are the local trends from the seasonal-trend  
 1311 decomposition analysis.

1312

1313

1314

1315

1316

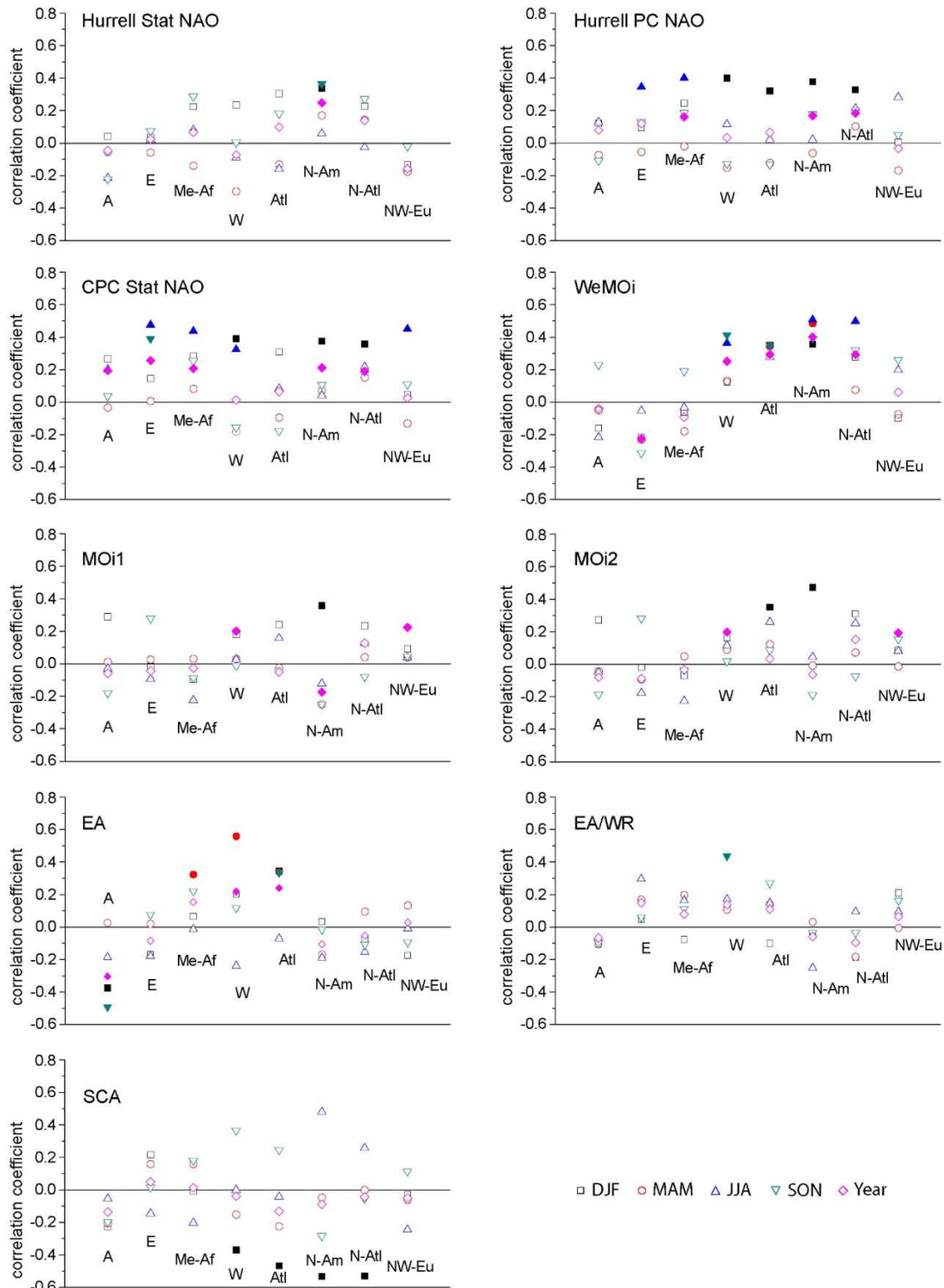
1317

1318

1319

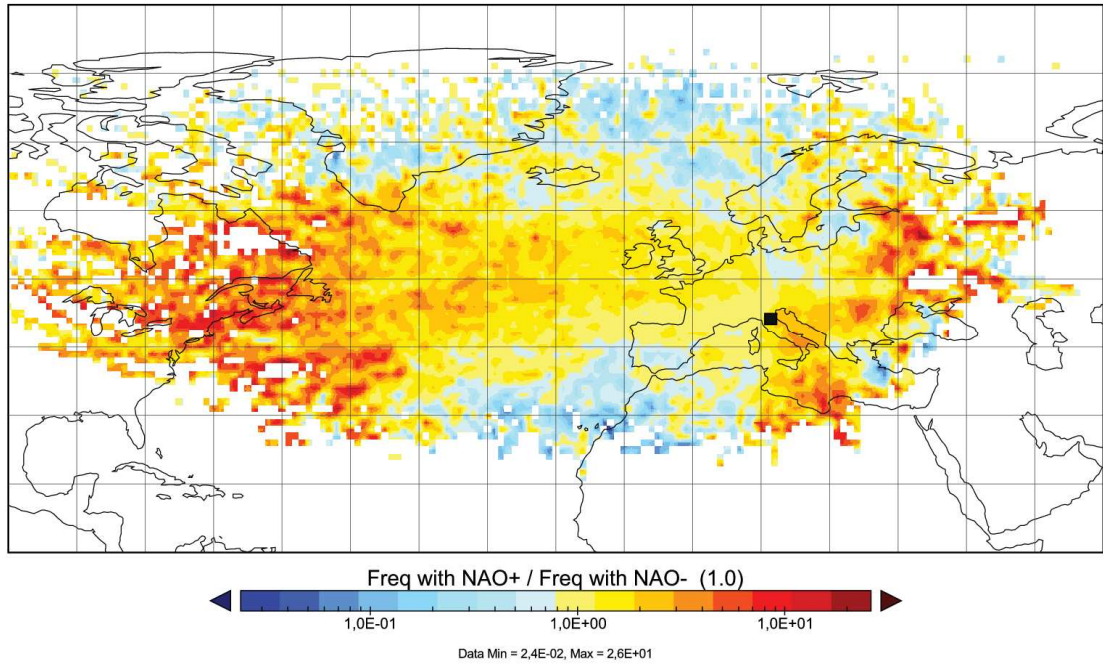
1320

1321

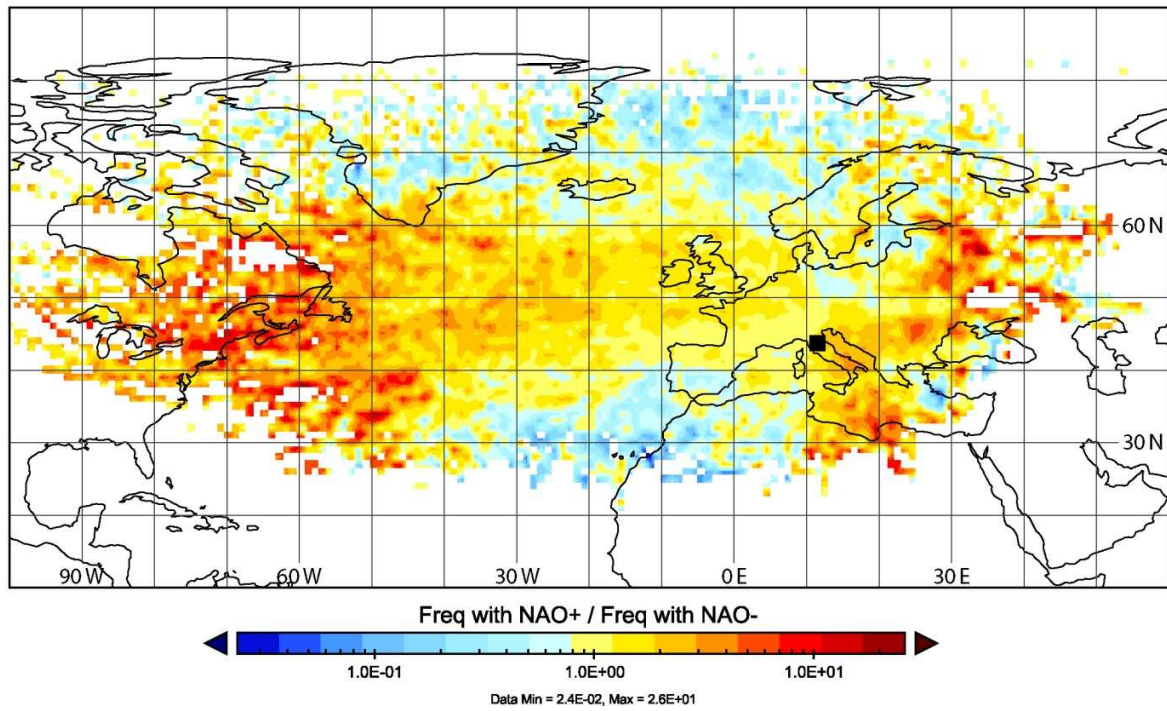


1322

1323 **Figure 8.** Spearman correlation coefficients between the frequency of occurrence of the different  
 1324 teleconnection indices and air flow types by season and for the full year. Filled symbols indicate  
 1325 significant correlations ( $p < 0.01$  significance level).  
 1326



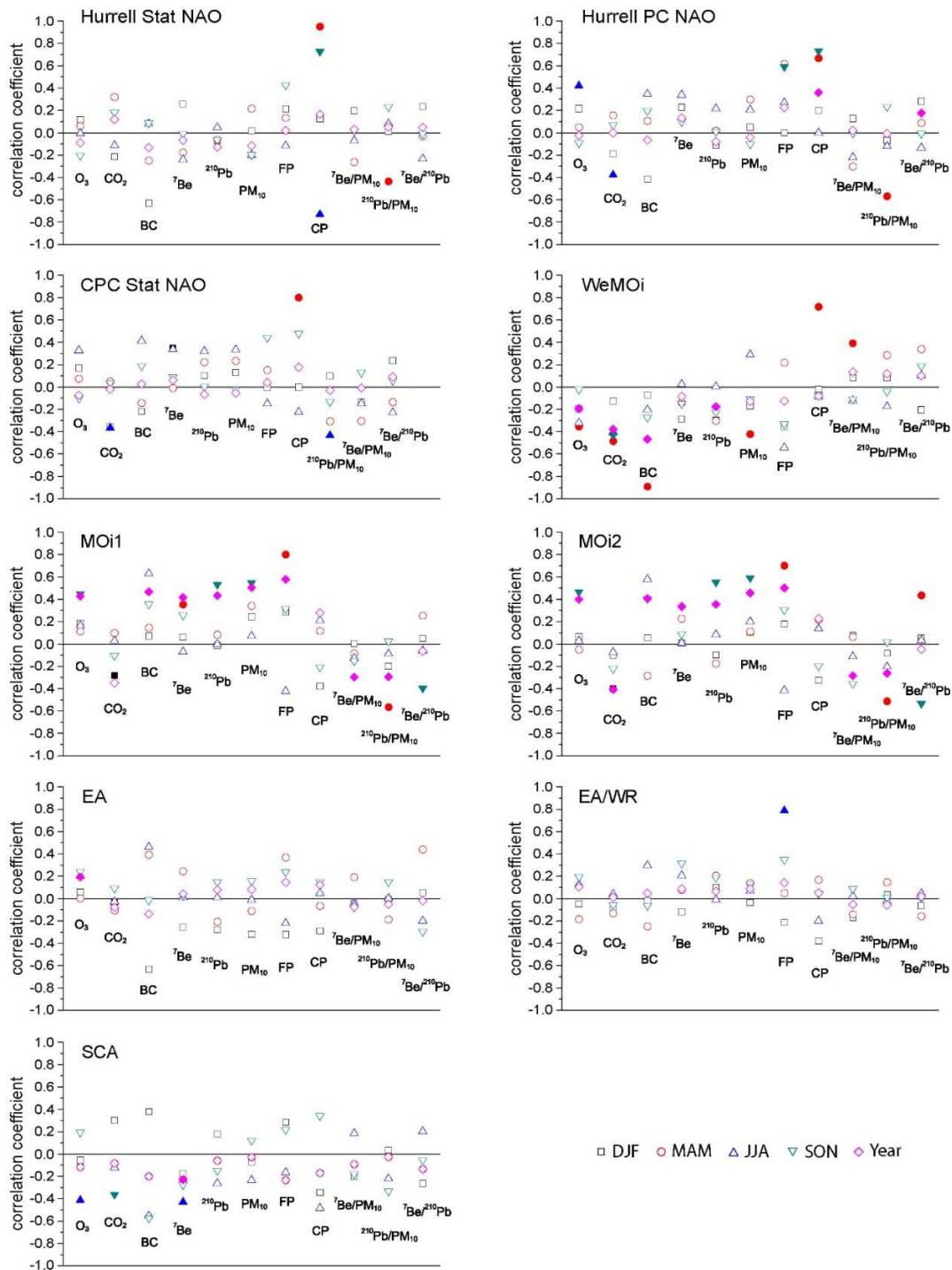
1327



1328

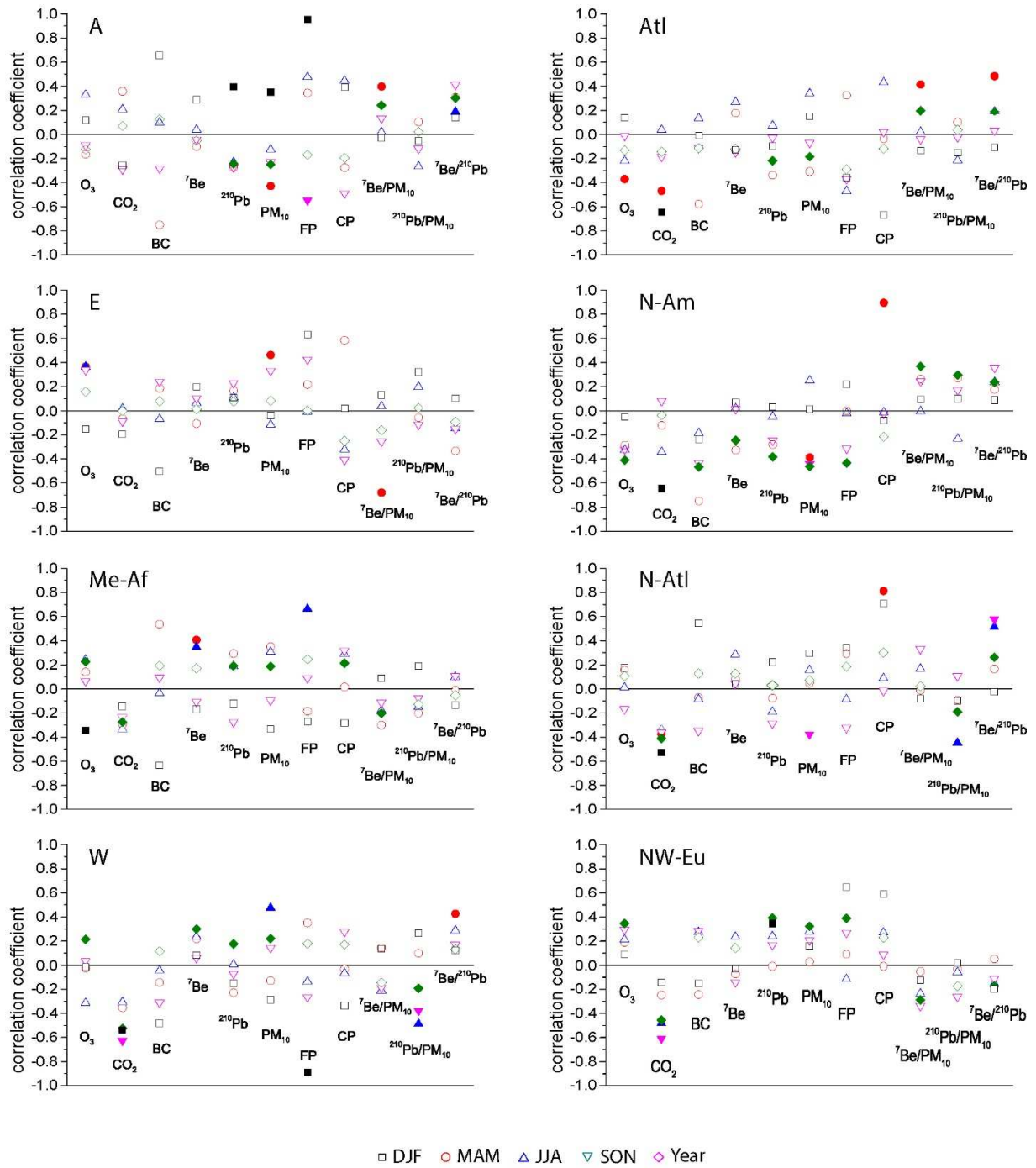
1329 **Figure 9.** Ratio of residence time of air parcels reaching Mt. Cimone in the positive and negative  
 1330 phase of Hurrell Stat NAO (NAOi higher than +0.5 and lower than -0.5, respectively) in the  
 1331 extended winter DJFM period. The black dot indicates the position of Mt. Cimone.  
 1332

1333



1334

1335 **Figure 10.** Spearman correlation coefficients between the teleconnection indices and the  
 1336 monthly medians of variables by season and for the full year. Filled symbols indicate significant  
 1337 correlations ( $p < 0.01$  significance level) letters indicate the variables:  $O_3$  = ozone,  $CO_2$  = carbon  
 1338 dioxide, BC = black-carbon,  ${}^7Be$ ,  ${}^{210}Pb$ ,  $PM_{10}$ , FP = fine particles, CP = coarse particles,  
 1339  ${}^7Be/PM_{10}$ ,  ${}^{210}Pb/PM_{10}$ ,  ${}^7Be/{}^{210}Pb$ .  
 1340



1341

1342 **Figure 11.** Same as Figure 10 but for the correlation between the frequency of occurrence of air  
1343 flow types and the monthly medians of variables.  
1344  
1345

Journal Pre-proof

## Author contributions

Use this form to specify the contribution of each author of your manuscript. A distinction is made between five types of contributions: Conceived and designed the analysis; Collected the data; Contributed data or analysis tools; Performed the analysis; Wrote the paper.

For each author of your manuscript, please indicate the types of contributions the author has made. An author may have made more than one type of contribution. Optionally, for each contribution type, you may specify the contribution of an author in more detail by providing a one-sentence statement in which the contribution is summarized. In the case of an author who contributed to performing the analysis, the author's contribution for instance could be specified in more detail as 'Performed the computer simulations', 'Performed the statistical analysis', or 'Performed the text mining analysis'.

If an author has made a contribution that is not covered by the five pre-defined contribution types, then please choose 'Other contribution' and provide a one-sentence statement summarizing the author's contribution.

**Manuscript title:** Advection pathways at the Mt. Cimone WMO-GAW station: seasonality, trends, and influence on atmospheric composition

**Author 1:** Erika Brattich

- Conceived and designed the analysis**  
Specify contribution in more detail (optional; no more than one sentence)
- Collected the data**  
Specify contribution in more detail (optional; no more than one sentence)
- Contributed data or analysis tools**  
Specify contribution in more detail (optional; no more than one sentence)
- Performed the analysis**  
Specify contribution in more detail (optional; no more than one sentence)
- Wrote the paper**  
Specify contribution in more detail (optional; no more than one sentence)
- Other contribution**  
Specify contribution in more detail (required; no more than one sentence)

**Author 2:** José Antonio Garcia Orza

- Conceived and designed the analysis**  
Specify contribution in more detail (optional; no more than one sentence)
- Collected the data**  
Specify contribution in more detail (optional; no more than one sentence)
- Contributed data or analysis tools**  
Specify contribution in more detail (optional; no more than one sentence)
- Performed the analysis**  
Specify contribution in more detail (optional; no more than one sentence)
- Wrote the paper**  
Specify contribution in more detail (optional; no more than one sentence)
- Other contribution**  
Specify contribution in more detail (required; no more than one sentence)

**Author 3:** Paolo Cristofanelli

- Conceived and designed the analysis**  
Specify contribution in more detail (optional; no more than one sentence)
- Collected the data**  
Specify contribution in more detail (optional; no more than one sentence)
- Contributed data or analysis tools**  
Specify contribution in more detail (optional; no more than one sentence)
- Performed the analysis**  
Specify contribution in more detail (optional; no more than one sentence)
- Wrote the paper**  
Specify contribution in more detail (optional; no more than one sentence)
- Other contribution**  
Specify contribution in more detail (required; no more than one sentence)

**Author 4:** Paolo Bonasoni

- Conceived and designed the analysis**  
Specify contribution in more detail (optional; no more than one sentence)
- Collected the data**  
Specify contribution in more detail (optional; no more than one sentence)
- Contributed data or analysis tools**  
Specify contribution in more detail (optional; no more than one sentence)
- Performed the analysis**  
Specify contribution in more detail (optional; no more than one sentence)
- Wrote the paper**  
Specify contribution in more detail (optional; no more than one sentence)
- Other contribution**  
Specify contribution in more detail (required; no more than one sentence)

**Author 5:** Angela Marinoni

- Conceived and designed the analysis**  
Specify contribution in more detail (optional; no more than one sentence)
- Collected the data**  
Specify contribution in more detail (optional; no more than one sentence)
- Contributed data or analysis tools**  
Specify contribution in more detail (optional; no more than one sentence)
- Performed the analysis**  
Specify contribution in more detail (optional; no more than one sentence)
- Wrote the paper**  
Specify contribution in more detail (optional; no more than one sentence)
- Other contribution**  
Specify contribution in more detail (required; no more than one sentence)

**Author 6:** Laura Tositti

- Conceived and designed the analysis**  
Specify contribution in more detail (optional; no more than one sentence)
- Collected the data**  
Specify contribution in more detail (optional; no more than one sentence)
- Contributed data or analysis tools**  
Specify contribution in more detail (optional; no more than one sentence)
- Performed the analysis**  
Specify contribution in more detail (optional; no more than one sentence)
- Wrote the paper**  
Specify contribution in more detail (optional; no more than one sentence)
- Other contribution**  
Specify contribution in more detail (required; no more than one sentence)

**Author 7:**

- Conceived and designed the analysis**  
Specify contribution in more detail (optional; no more than one sentence)
- Collected the data**  
Specify contribution in more detail (optional; no more than one sentence)
- Contributed data or analysis tools**  
Specify contribution in more detail (optional; no more than one sentence)
- Performed the analysis**  
Specify contribution in more detail (optional; no more than one sentence)
- Wrote the paper**  
Specify contribution in more detail (optional; no more than one sentence)
- Other contribution**  
Specify contribution in more detail (required; no more than one sentence)

**Author 8:**

- Conceived and designed the analysis**  
Specify contribution in more detail (optional; no more than one sentence)
- Collected the data**  
Specify contribution in more detail (optional; no more than one sentence)
- Contributed data or analysis tools**  
Specify contribution in more detail (optional; no more than one sentence)
- Performed the analysis**  
Specify contribution in more detail (optional; no more than one sentence)
- Wrote the paper**  
Specify contribution in more detail (optional; no more than one sentence)
- Other contribution**  
Specify contribution in more detail (required; no more than one sentence)

**Author 9:** Enter author name

- Conceived and designed the analysis**  
Specify contribution in more detail (optional; no more than one sentence)
- Collected the data**  
Specify contribution in more detail (optional; no more than one sentence)
- Contributed data or analysis tools**  
Specify contribution in more detail (optional; no more than one sentence)
- Performed the analysis**  
Specify contribution in more detail (optional; no more than one sentence)
- Wrote the paper**  
Specify contribution in more detail (optional; no more than one sentence)
- Other contribution**  
Specify contribution in more detail (required; no more than one sentence)

**Author 10:** Enter author name

- Conceived and designed the analysis**  
Specify contribution in more detail (optional; no more than one sentence)
- Collected the data**  
Specify contribution in more detail (optional; no more than one sentence)
- Contributed data or analysis tools**  
Specify contribution in more detail (optional; no more than one sentence)
- Performed the analysis**  
Specify contribution in more detail (optional; no more than one sentence)
- Wrote the paper**  
Specify contribution in more detail (optional; no more than one sentence)
- Other contribution**  
Specify contribution in more detail (required; no more than one sentence)